Stability analysis of deep-water waves on a linear shear current using unsteady conformal mapping

Sunao Murashige[1],[†] and Wooyoung Choi[2]

[1]Department of Mathematics and Informatics, Ibaraki University, Mito, Ibaraki, 310-8512, Japan

[2]Department of Mathematical Sciences, New Jersey Institute of Technology, Newark, NJ 07102-1982, USA

This paper describes linear stability analysis of the two-dimensional steady motion of periodic deep-water waves with symmetric non-overhanging profiles propagating on a linear shear current, namely a vertically sheared current with constant vorticity. In order to investigate numerically with high accuracy the stability of large-amplitude waves, we adopt a formulation using conformal mapping, in which the time-varying water surface is always mapped onto the real axis of a complex plane. This formulation allows us to apply numerical methods developed for large-amplitude irrotational waves without a shear current directly to the present problem, and reduces the linear stability problem to a generalized eigenvalue problem. Numerical solutions describe both super- and sub-harmonic instabilities of the periodic waves for a wide range of wave amplitudes and clarify how the behaviours of dominant eigenvalues change with the strength of the shear current. In particular, it is shown that, even in the presence of a linear shear current, the steady periodic waves lose stability due to superharmonic disturbances at the wave amplitude where the wave energy attains an extremum, similarly to the case of irrotational waves without a shear current. It is also found that re-stabilization with an increase in wave amplitude characterizes subharmonic instability for weak shear currents, but the re-stabilization disappears for strong shear currents.

1. Introduction

The interaction of surface waves with a vertically sheared current plays an important role in the ocean (see a review by Peregrine (1976)). For example, Banner & Phillips (1974), Banner & Song (2002) and Yao & Wu (2005) demonstrated that the presence of a shear current varying with depth affects the breaking limit of surface waves. See also the experimental studies of current–wave interactions by Thomas (1981, 1990) and Swan, Cummins & James (2001).

The present work considers stability of the two-dimensional periodic motion of steady deep-water waves of symmetric profile on a linear shear current with the

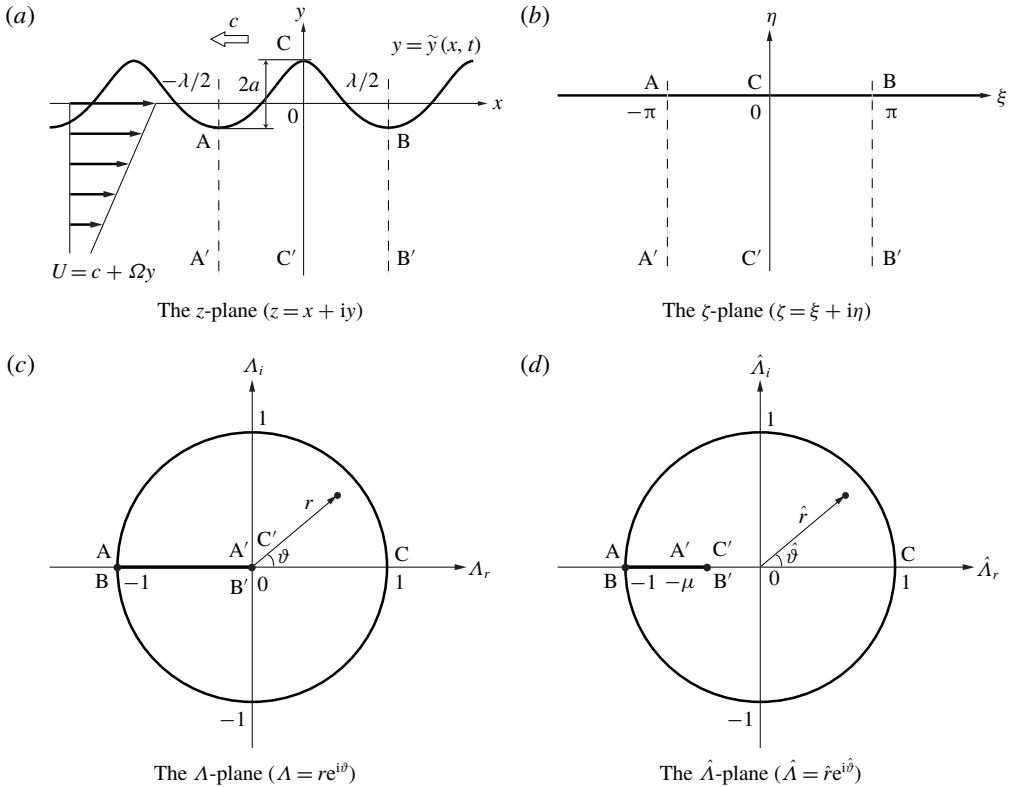† Email address for correspondence: sunao.murashige.sci@vc.ibaraki.ac.jp

FIGURE 1. Deep-water waves on a linear shear current and conformal mapping of the flow domain. The mapping functions among the ζ-, Λ- and $\hat{\Lambda}$-planes are given by (2.16). U: the horizontal velocity of the shear current in the frame of reference moving to the left with the wave speed c, Ω: the shear strength, λ: the wavelength and a: the wave amplitude (one half of the crest-to-trough height).

horizontal velocity distribution $U(y) = c + \Omega y$ in the frame of reference moving to the left with the wave speed c, where the shear strength Ω is a constant, as shown in figure 1(*a*). Note that waves for $\Omega > 0$ and $\Omega < 0$ are referred to as upstream and downstream propagating waves, respectively.

Since the vorticity in a two-dimensional incompressible and inviscid flow is conserved and the vorticity of a linear shear current is constant $(= -\Omega)$, any perturbations must be irrotational. Therefore, we can formulate the present problem within the framework of potential flow theory and introduce the complex velocity potential for perturbed wave motions. It should be noted that, although the waves of interest are irrotational even for $\Omega \neq 0$, in this paper, only the waves without a shear current are referred to as irrotational waves $(\Omega = 0)$. On the basis of this formulation, the full Euler system has been numerically solved by Simmen & Saffman (1985), Teles da Silva & Peregrine (1988) and Vanden-Broeck (1996) for steady waves, and by Choi (2009) and Moreira & Chacaltana (2015) for unsteady waves. It has been known that the limiting form of steady waves of symmetric profile can have a corner at the wave crest with an inner angle of 120° which is independent of the shear strength Ω (Milne-Thomson 1968, p. 403, §14.50), similarly to the case of irrotational waves $(\Omega = 0)$.

Steady wave solutions for $\Omega \neq 0$ are determined by two dimensionless parameters, $\Omega_* = \Omega/\sqrt{gk}$ and the wave steepness $a_* = ak$, where g, k and a denote the gravitational acceleration, the wavenumber and the wave amplitude (one half of the crest-to-trough height), respectively. In this work, we numerically investigate the linear stability of non-overhanging periodic waves for $-3 \leqslant \Omega_* \leqslant 0.6$ and a wide range of the wave steepnesses a_*, for which instabilities due to super- and sub-harmonic disturbances are observed. For upstream propagating waves ($\Omega > 0$), while overhanging wave profiles appear for large values of Ω_* (Simmen & Saffman 1985; Teles da Silva & Peregrine 1988; Vanden-Broeck 1996; Dyachenko & Hur 2019*a,b*), a spectral method for computation of the steady solutions requires a number N of Fourier modes of the order of 10^4, which is much greater than that in our numerical stability analysis, typically, $N \leqslant 2^9 (= 512)$.

In the absence of a shear current, the linear stability of steady solutions of the full Euler system for finite-amplitude irrotational waves ($\Omega = 0$) has been studied extensively by, for example, Longuet-Higgins (1978*a,b*), McLean (1982) and Tanaka (1983) for periodic gravity waves; Zhang & Melville (1987) for gravity–capillary waves; Chen & Saffman (1985) and Tiron & Choi (2012) for capillary waves; Tanaka (1986) for solitary waves. In particular, Longuet-Higgins (1978*b*) and Tanaka (1983) found numerically two typical behaviours of eigenvalues of the linearized system for small disturbances to steady wave solutions, (i) a 'bubble of instability' due to subharmonic disturbances, as shown in figure 8(*a*1) and (ii) the 'Tanaka instability' due to superharmonic disturbances, as shown in figure 5(*a*), respectively (MacKay & Saffman 1986). Here sub- and super-harmonic disturbances are those with horizontal scale longer and shorter than steady waves, respectively. In this work, the focus is on how these two instabilities change with the shear strength Ω.

In the presence of a linear shear current, weakly nonlinear theories for small-amplitude waves have been first developed. For steady waves, asymptotic theories were presented by Benjamin (1962) and Miroshnikov (2002) for weakly and strongly nonlinear solitary waves, respectively, Simmen & Saffman (1985) for deep-water waves and Hsu *et al.* (2016) for gravity–capillary waves on water of finite depth. For unsteady waves, Freeman & Johnson (1970) and Choi (2003) obtained the weakly nonlinear Korteweg–de Vries equation and a strongly nonlinear long wave model for shallow-water waves, respectively, while Thomas, Kharif & Manna (2012) derived a nonlinear Schrödinger (NLS) equation for the envelope of periodic waves on water of finite and infinite depth. Using the NLS equation, Thomas *et al.* (2012) and Francius & Kharif (2017) investigated the effect of a shear current on the Benjamin–Feir instability, which occurs at relatively small amplitudes, and pointed out that the deep-water limit of coupling between the mean flow and the background vorticity is essential for the evaluation of the stability of deep-water waves.

A few attempts have been made previously for numerical investigation of the linear stability of finite-amplitude waves on a linear shear current ($\Omega \neq 0$), including Okamura & Oikawa (1989) and Francius & Kharif (2017), who used the full Euler system for periodic waves on water of finite depth. Okamura & Oikawa (1989) examined the three-dimensional instability of two-dimensional steady waves, similarly to McLean (1982) for irrotational waves ($\Omega = 0$). Francius & Kharif (2017) investigated two-dimensional instability for a wide range of the shear strengths, Ω, and compared the results with their weakly nonlinear theory (Thomas *et al.* 2012). In particular, Francius & Kharif (2017) discovered re-stabilization of the Benjamin–Feir instability with a change of Ω for upstream propagating waves ($\Omega > 0$), which may be dominated by new bands of instability. Notice that the propagation direction of

waves in this work is opposite to that in Francius & Kharif (2017) and so is the sign of Ω for upstream and downstream propagating waves.

Saffman (1985) analytically proved, using Zakharov's Hamiltonian formulation for $\Omega = 0$ (Zakharov 1968), that, at the critical point of the Tanaka superharmonic instability, exchange of stability occurs and the wave energy is an extremum as a function of wave amplitude, as numerically shown by Tanaka (1983, 1985). Wahlén (2007) derived a canonical Hamiltonian system for water waves on a linear shear current by generalizing Zakharov's formulation with a suitable choice of canonical variables. Sato & Yamada (2019) pointed out that translational symmetry in a canonical Hamiltonian system is essential in the Tanaka instability, and analytically predicted from the result by Wahlén (2007) that the same type of instability can occur even in the presence of a linear shear current.

In Francius & Kharif (2017), the maximum wave steepness is $ka = 0.2$ for $-0.6 \leqslant \Omega/\sqrt{gk} \leqslant 1$, which is much less than $ka \simeq 0.4292$, at which the Tanaka superharmonic instability for $\Omega = 0$ occurs. Thus, their stability results are limited to moderate wave steepness, mainly due to slow convergence of their numerical methods. Furthermore, no stability analysis has been presented for superharmonic disturbances in previous studies. In this work, we apply one of the conformal mapping techniques to the linear stability analysis of large-amplitude waves in §4, and present some numerical examples of both sub- and super-harmonic instabilities in §5.

To compute large-amplitude steady waves, the hodograph transformation has been widely used. Its original idea is to interchange the dependent and independent variables such that spatial coordinates are functions of the velocity potential ϕ and the streamfunction ψ. Its major advantage is that the water surface is located on the real axis, or $\psi = 0$ in the complex function $f (= \phi + i\psi)$-plane where the flow domain is conformally mapped. On the other hand, for unsteady waves, the streamfunction ψ is not constant and vary with time on the free surface (Longuet-Higgins 1978*a,b*). Therefore, to study the stability of large-amplitude waves, we should generalize the idea of the hodograph transformation to unsteady waves. Such a generalization has been explored for unsteady waves to find a transformation, where the unknown location of the free surface is mapped on the real axis $\eta = 0$ of a complex plane, or the $\zeta (= \xi + i\eta)$-plane, which is guaranteed by the Riemann mapping theory. It has been shown that the time-dependent transformation can be found by solving the nonlinear evolution equations and this idea has been applied to various water wave problems by Ovshannikov (1974), Dyachenko, Zakharov & Kuznetsov (1996), Choi & Camassa (1999), Chalikov & Sheinin (2005) and Murashige & Choi (2017) for $\Omega = 0$, and by Ruban (2008), Choi (2009) and Dyachenko & Hur (2019*a,b*) for $\Omega \neq 0$. The same formulation has been also used for stability analysis by Tiron & Choi (2012) for pure capillary waves and Dosaev, Troitskaya & Shishina (2017) for the Benjamin–Feir instability of deep-water gravity waves on a linear shear current. In this work, we apply the idea of this time-dependent transformation to study the linear stability of large-amplitude waves.

The paper is organized as follows. Formulation of the problem using conformal mapping is presented in §2. Computed results for steady waves of symmetric profile are shown in §3. The method of linear stability analysis following the Floquet theory in the conformally mapped planes is shown in §4. Numerical examples of linear stability analysis for super- and sub-harmonic disturbances are summarized and discussed in §5. Section 6 concludes this work.

2. Formulation of the problem

2.1. *Formulation in the physical plane*

Consider the stability of the periodic steady motion of deep-water gravity waves progressing to the left in permanent form with constant speed c on a linear shear current, as shown in figure 1(*a*). The profile of the periodic steady waves is assumed to be symmetric with respect to the vertical line passing through the wave crest. It is also assumed that the fluid motion is two-dimensional in the vertical cross-section (x, y) along the propagation direction of the waves, and that the fluid is inviscid and incompressible. The origin is placed such that the wave profile $y = \tilde{y}(x, t)$ satisfies the zero mean level condition

$$\int_0^\lambda \tilde{y}(x, t)\, \mathrm{d}x = 0, \tag{2.1}$$

where λ is the wavelength and t denotes the time.

It is convenient to formulate the problem in the frame of reference moving with the waves so that the horizontal velocity of a linear shear current is given by $U = c + \Omega y$ with constant Ω. Then, the fluid velocity vector $\boldsymbol{U}$ can be written as

$$\boldsymbol{U} = \begin{pmatrix} U \\ V \end{pmatrix} = \begin{pmatrix} \Omega y \\ 0 \end{pmatrix} + \begin{pmatrix} u \\ v \end{pmatrix}, \tag{2.2}$$

with the bottom boundary condition

$$\begin{pmatrix} u \\ v \end{pmatrix} \to \begin{pmatrix} c \\ 0 \end{pmatrix} \quad \text{as } y \to -\infty. \tag{2.3}$$

In the case of no wave motion, $u = c$ and $v = 0$. From conservation of vorticity for two-dimensional flows, as the vorticity remains constant $(= -\Omega)$ if it is initially constant, the perturbed wave motion given by (u, v) must be irrotational. Thus we can introduce the complex velocity potential f defined by

$$f(z, t) = \phi(x, y, t) + \mathrm{i}\psi(x, y, t) \quad \text{with} \quad \frac{\partial f}{\partial z} = w = u - \mathrm{i}v, \tag{2.4a,b}$$

where $z = x + \mathrm{i}y$ and $w = u - \mathrm{i}v$ denote the complex coordinate and the complex velocity, respectively. In addition, from the mass conservation law given by $U_x + V_y = 0$, there exists a streamfunction Ψ defined by

$$U = \Psi_y \quad \text{and} \quad V = -\Psi_x. \tag{2.5a,b}$$

From (2.2) and (2.4), Ψ is related to $\psi = \mathrm{Im}\{f\}$ by

$$\Psi = \tfrac{1}{2}\Omega y^2 + \psi. \tag{2.6}$$

When physical variables are non-dimensionalized, with respect to c and $k(= 2\pi/\lambda)$, as

$$z_* = kz, \quad t_* = ckt, \quad f_* = \frac{f}{(c/k)}, \quad \tilde{y}_* = k\tilde{y}, \tag{2.7a-d}$$

the following dimensionless parameters appear in the problem:

$$a_* = ka, \quad \Omega_* = \frac{\Omega}{\sqrt{gk}}, \quad c_* = \frac{c}{\sqrt{g/k}}, \tag{2.8a-c}$$

where a denotes the wave amplitude (one half of the crest-to-trough height) and $a_* = ka$ is the wave steepness. Henceforth the asterisks for dimensionless variables will be omitted for brevity.

The boundary conditions at the water surface $y = \tilde{y}(x, t)$ are given, from the kinematic condition, by

$$\tilde{y}_t + \left(\phi_x + \frac{\Omega}{c}\tilde{y} \right) \tilde{y}_x = \phi_y \quad \text{at } y = \tilde{y}(x, t), \tag{2.9}$$

and, from the dynamic condition, by

$$\phi_t + \frac{1}{c^2}\tilde{y} + \frac{1}{2}(\phi_x{}^2 + \phi_y{}^2) + \frac{\Omega}{c}(\tilde{y}\phi_x - \psi) = B(t) \quad \text{at } y = \tilde{y}(x, t), \tag{2.10}$$

where an arbitrary function $B(t)$ can be absorbed into ϕ. Also the bottom boundary condition (2.3) as $y \to -\infty$ can be rewritten as

$$\frac{\partial f}{\partial z} = \phi_x + \mathrm{i}\psi_x \to 1 \quad \text{as } y \to -\infty. \tag{2.11}$$

2.2. *Unsteady conformal mapping of the flow domain*

For linear stability analysis of large-amplitude steady waves, we introduce a conformal mapping technique (Dyachenko *et al.* 1996; Ruban 2008; Choi 2009; Tiron & Choi 2012; Dosaev *et al.* 2017; Murashige & Choi 2017; Dyachenko & Hur 2019*a*,*b*) which maps the flow domain onto the lower half $\eta < 0$ of the ζ-plane ($\zeta = \xi + \mathrm{i}\eta$) or the unit disk $|\hat{\Lambda}| < 1$ in the $\hat{\Lambda}$-plane ($\hat{\Lambda} = \hat{r}\mathrm{e}^{\mathrm{i}\hat{\vartheta}}$), as shown in figure 1. The time-varying water surface is always mapped onto the real axis $\eta = 0$ in the ζ-plane or the unit circle $\hat{\Lambda} = \mathrm{e}^{\mathrm{i}\hat{\vartheta}}$ in the $\hat{\Lambda}$-plane.

Numerical computation of large-amplitude waves close to the limiting waves with a corner at the wave crest requires high resolution in space near the crest, and some auxiliary conformal mappings for it has been proposed (Tanaka 1983; Murashige & Tanaka 2015; Lushnikov, Dyachenko & Silantyev 2017). For irrotational waves ($\Omega = 0$), Tanaka (1983) controlled the spatial resolution near the wave crest by conformally mapping the flow domain onto the unit disk in the $\hat{\Lambda}$-plane and succeeded in numerically capturing the Tanaka superharmonic instability occurring at a large amplitude ($ka \simeq 0.4292$). We apply this idea to the present problem for numerical investigation of the linear stability of large-amplitude waves subject to superharmonic disturbances.

2.2.1. *The ζ-plane for unsteady wave motion*

In the ζ-plane ($\zeta = \xi + \mathrm{i}\eta$), we choose $z = z(\zeta, t)$ and $f = f(\zeta, t)$ as dependent variables. Then, the mapping function between the z- and ζ-planes is given by a solution $z = z(\zeta, t)$ of the problem. The flow domain is conformally mapped onto the lower half $\eta < 0$, as shown in figure 1(*b*), and the free surface boundary conditions, namely the kinematic and dynamic conditions, at the water surface $\eta = 0$ are given, respectively, by

$$x_\xi y_t - y_\xi x_t = -\left(\psi_\xi + \frac{\Omega}{c}yy_\xi \right) \quad \text{at } \eta = 0, \tag{2.12}$$

and

$$\phi_t - \frac{\phi_\xi}{J}(x_\xi x_t + y_\xi y_t) + \frac{1}{c^2}y + \frac{1}{2J}(\phi_\xi{}^2 - \psi_\xi{}^2) + \frac{\Omega}{c}\left(\frac{\phi_\xi}{J}yx_\xi - \psi\right) = B(t) \quad \text{at } \eta = 0,$$

(2.13)

where J is defined by

$$J = \frac{\partial(x, y)}{\partial(\xi, \eta)} = x_\xi{}^2 + y_\xi{}^2.$$

(2.14)

The bottom boundary condition (2.11) is satisfied with

$$z \to \zeta \quad \text{and} \quad f \to \zeta \quad \text{as } \eta \to -\infty.$$

(2.15a,b)

Notice that Tiron & Choi (2012) adopted alternative forms of the free surface boundary conditions given by (A 2) and (A 3) including the Hilbert transform, instead of (2.12) and (2.13), for linear stability analysis of capillary waves (see appendix A). In this work, we use (2.12) and (2.13) which do not require direct evaluation of the Hilbert transform, but the stability results from the two different forms would be identical.

2.2.2. *The $\hat{\Lambda}$-plane for 2π-periodic wave motion*

For 2π-periodic wave motions, it is convenient to further map the flow domain onto the unit disk in the $\hat{\Lambda}$-plane, as shown in figure 1(*d*), where the spatial resolution at the water surface can be controlled for accurate computation of large-amplitude waves (Tanaka 1983; Longuet-Higgins & Tanaka 1997). The $\hat{\Lambda}$-plane is obtained by the following two transformations through the Λ-plane shown in figure 1(*c*):

$$\Lambda = e^{-i\zeta} \quad \text{and} \quad \Lambda = \frac{\hat{\Lambda} + \mu}{1 + \mu\hat{\Lambda}} \quad (0 \leqslant \mu < 1).$$

(2.16a,b)

Branch cuts are set to $-\infty < \Lambda \leqslant 0$ and $-1/\mu \leqslant \hat{\Lambda} \leqslant -\mu$ along the real axes in the Λ- and $\hat{\Lambda}$-planes, respectively, such that $\log \Lambda$ is uniquely defined. The water surface is mapped onto the unit circle $\Lambda = e^{i\vartheta}$ or $\hat{\Lambda} = e^{i\hat{\vartheta}}$, and the argument ϑ in the Λ-plane is related to ξ and the argument $\hat{\vartheta}$ in the $\hat{\Lambda}$-plane at the water surface, respectively, as

$$\vartheta = -\xi \quad \text{and} \quad \tan\vartheta = \frac{(1 - \mu^2)\sin\hat{\vartheta}}{2\mu + (1 + \mu^2)\cos\hat{\vartheta}} \quad (-\pi \leqslant \xi, \vartheta, \hat{\vartheta} \leqslant \pi).$$

(2.17a,b)

The wave crest $\xi = 0$ and trough $\xi = \pm\pi$ of 2π-periodic steady waves are mapped onto $\vartheta = \hat{\vartheta} = 0$ and $\vartheta = \hat{\vartheta} = \mp\pi$, respectively. When the water surface $\hat{\Lambda} = e^{i\hat{\vartheta}}$ is divided into a finite number of equal intervals in the $\hat{\Lambda}$-plane, the spatial resolution near the wave crest in the physical plane (the z-plane) increases with the parameter $\mu \in [0, 1)$ in the mapping function (2.16). Also, the bottom $y \to -\infty$ is mapped onto $\Lambda = 0$ or $\hat{\Lambda} = -\mu$.

Similarly to the ζ-plane, we adopt z and f as dependent variables in the $\hat{\Lambda}$-plane. We write these dependent variables z and f in the $\hat{\Lambda}$-plane as $z = z(\hat{\Lambda}, t)$ and $f = f(\hat{\Lambda}, t)$, respectively, instead of $z = z(\zeta(\hat{\Lambda}), t)$ and $f = f(\zeta(\hat{\Lambda}), t)$, for convenience. The

free surface boundary conditions, namely the kinematic and dynamic conditions, at the water surface $\hat{\Lambda} = e^{i\hat{\vartheta}}$ are given, respectively, by

$$x_{\hat{\vartheta}} y_t - y_{\hat{\vartheta}} x_t = -\left(\psi_{\hat{\vartheta}} + \frac{\Omega}{c} y y_{\hat{\vartheta}}\right) \quad \text{at } \hat{\Lambda} = e^{i\hat{\vartheta}}, \tag{2.18}$$

and

$$\phi_t - \frac{\phi_{\hat{\vartheta}}}{\hat{J}}(x_{\hat{\vartheta}} x_t + y_{\hat{\vartheta}} y_t) + \frac{1}{c^2} y + \frac{1}{2\hat{J}}(\phi_{\hat{\vartheta}}^2 - \psi_{\hat{\vartheta}}^2) + \frac{\Omega}{c}\left(\frac{\phi_{\hat{\vartheta}}}{\hat{J}} y x_{\hat{\vartheta}} - \psi\right) = B(t) \quad \text{at } \hat{\Lambda} = e^{i\hat{\vartheta}}, \tag{2.19}$$

where $-\pi \leqslant \hat{\vartheta} \leqslant \pi$ and $\hat{J}$ is defined by

$$\hat{J} = x_{\hat{\vartheta}}^2 + y_{\hat{\vartheta}}^2. \tag{2.20}$$

The bottom boundary condition (2.15) becomes

$$z(\hat{\Lambda}) \to i \log \Lambda(\hat{\Lambda}) \quad \text{and} \quad f(\hat{\Lambda}) \to i \log \Lambda(\hat{\Lambda}) \quad \text{as } \hat{\Lambda} \to -\mu, \tag{2.21a,b}$$

where $\Lambda = \Lambda(\hat{\Lambda})$ is given by (2.16).

3. Steady waves of symmetric profile

We write steady solutions of 2π-periodic waves of symmetric profile as $z = z_0(\zeta)$ and $f = f_0(\zeta)$ in the ζ-plane while $z = z_0(\hat{\Lambda})$ and $f = f_0(\hat{\Lambda})$ in the $\hat{\Lambda}$-plane. In their computations for $\Omega = 0$, Tanaka (1983) and Longuet-Higgins & Tanaka (1997) adopted γ, as one of parameters for steady waves, which is defined by

$$\gamma = 1 - q_{crest}/q_{trough}, \tag{3.1}$$

where q_{crest} and q_{trough} denote the fluid velocity at the wave crest and trough in the frame of reference moving with steady waves, respectively. For a wide range of Ω, this parameter $\gamma \in [0, 1]$ monotonically increases with the wave steepness ka. The maximum wave steepness ka of the limiting wave changes with the shear strength Ω, while the corresponding $\gamma = 1$ is invariant with respect to Ω considered in this work, as shown in figure 7. Then we use this parameter γ, instead of the wave steepness ka for the computations of steady waves for $\Omega \neq 0$.

3.1. *Boundary conditions*

In the ζ-plane, the kinematic condition (2.12) for steady waves is reduced to

$$\psi_{0\xi} = -\frac{\Omega}{c} y_0 y_{0\xi} \quad \text{or} \quad \psi_0 = -\frac{\Omega}{2c} y_0^2 + \text{constant} \quad \text{at } \eta = 0. \tag{3.2a,b}$$

Substituting this into the dynamic condition (2.13), we get

$$\left(\phi_{0\xi} + \frac{\Omega}{c} y_0 x_{0\xi}\right)^2 - J_0\left(B_0 - \frac{2}{c^2} y_0\right) = 0 \quad \text{at } \eta = 0, \tag{3.3}$$

where $-\pi \leqslant \xi \leqslant \pi$, B_0 is a real constant and

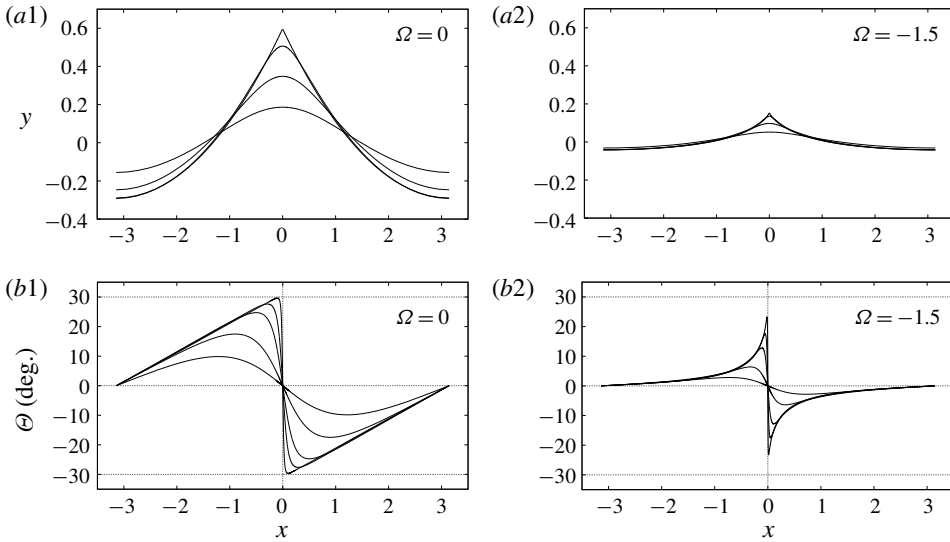$$J_0 = x_{0\xi}^2 + y_{0\xi}^2. \tag{3.4}$$

FIGURE 2. The wave profile $y = \tilde{y}_0(x)$ and the slope $\Theta = \tan^{-1}(d\tilde{y}_0/dx)$ of the surface of steady waves of symmetric profile for different values of γ. The parameter γ is defined by (3.1) ($N = 512$ and $\mu = 0.95$). (*a*1) $\Omega = 0$. (*a*2) $\Omega = -1.5$. (*b*1) $\Omega = 0$. (*b*2) $\Omega = -1.5$. (*a*) Wave profile $y = \tilde{y}_0(x)$ ($\gamma = 0.3, 0.5, 0.7$ and 0.95). (*b*) Slope Θ ($\gamma = 0.3, 0.5, 0.7, 0.8$ and 0.9).

In the $\hat{\Lambda}$-plane, (3.3) can be transformed using (2.17) to

$$\Gamma_1(\hat{\vartheta}) := \left(\phi_{0\hat{\vartheta}} + \frac{\Omega}{c} y_0 x_{0\hat{\vartheta}} \right)^2 - \hat{J}_0 \left(B_0 - \frac{2}{c^2} y_0 \right) = 0 \quad \text{at} \quad \hat{\Lambda} = e^{i\hat{\vartheta}}, \qquad (3.5)$$

where $-\pi \leqslant \hat{\vartheta} \leqslant \pi$ and

$$\hat{J}_0 = x_{0\hat{\vartheta}}{}^2 + y_{0\hat{\vartheta}}{}^2. \qquad (3.6)$$

The bottom boundary condition is given by (2.15) or (2.21) for $z = z_0$ and $f = f_0$.

3.2. Numerical solutions for steady waves

When the parameter γ defined by (3.1) and the shear strength Ω are given, we can compute steady wave solutions satisfying (2.21) and (3.5) in the $\hat{\Lambda}$-plane, similarly to Choi (2009) who computed the steady solutions in the ζ-plane. The computational method for steady waves in the $\hat{\Lambda}$-plane is summarized in appendix B.

Figures 2(*a*) and 2(*b*) show some computed results for the wave profile $y = \tilde{y}_0(x)$ and the slope $\Theta = \tan^{-1}(d\tilde{y}_0/dx)$ of the water surface for $\Omega = 0$ and -1.5, respectively, with $N = 512$ and $\mu = 0.95$. It is found that the wave crest at $x = 0$ approaches a corner of the inner angle $= 120°$ with increase of amplitude even for $\Omega \neq 0$ (Milne-Thomson 1968, p. 403, §14·50), while the rate of variation of the slope Θ near the crest significantly changes with the shear strength Ω.

Figure 3(*a*) compares some computed results for the wave speed c for $-3 \leqslant \Omega \leqslant 0.6$ and $0.01 \leqslant \gamma \leqslant 0.95$ ($N = 256$ and $\mu = 0.95$) with the weakly nonlinear solution (Simmen & Saffman 1985; Thomas *et al.* 2012; Hsu *et al.* 2016), which is correct to the second order in the wave steepness a, given by

$$c = c_0(1 + M_0 a^2) \quad \text{with} \quad M_0 = \tfrac{1}{8}(4 - 6\tilde{\Omega} + 6\tilde{\Omega}^2 - \tilde{\Omega}^3), \qquad (3.7a,b)$$
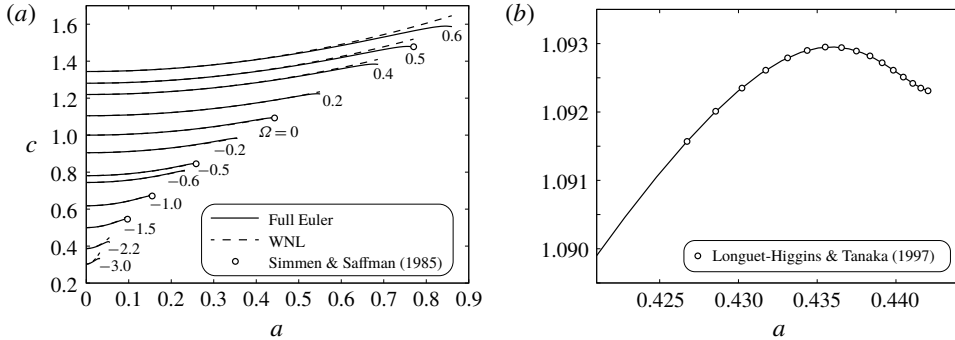
FIGURE 3. Variation of the wave speed c of steady waves of symmetric profile with the wave steepness a. Solid line ——: the computed results for the full Euler system using the present method ($N = 256$, $\mu = 0.95$, $0.01 \leqslant \gamma \leqslant 0.95$), dashed line $---$ in (a): the weakly nonlinear (denoted WNL) solution (3.7), circle $\circ$ in (a): the computed results for the limiting waves for $\Omega = 0.5$, 0, -0.5, -1 and -1.5 by Simmen & Saffman (1985, table 3 on p. 51), and circle $\circ$ in (b): the computed results by Longuet-Higgins & Tanaka (1997, table 2 on p. 53). Each numeral in (a) shows the value of shear strength Ω. (a) Wave speed c for $-3 \leqslant \Omega \leqslant 0.6$. ($b$) Wave speed c for large-amplitude irrotational waves ($\Omega = 0$).

where the linear wave speed c_0 satisfies the linear dispersion relation

$$c_0 = \frac{\Omega}{2} + \sqrt{1 + \left(\frac{\Omega}{2}\right)^2}, \tag{3.8}$$

and $\tilde{\Omega}(< 1)$ is defined by

$$\Omega = \frac{\tilde{\Omega}}{\sqrt{1 - \tilde{\Omega}}} \quad \text{or} \quad \tilde{\Omega} = \Omega\left(-\frac{\Omega}{2} + \sqrt{1 + \left(\frac{\Omega}{2}\right)^2}\right). \tag{3.9a,b}$$

See appendix C for the weakly nonlinear solutions of the NLS equation derived by Thomas *et al.* (2012).

Similarly to Simmen & Saffman (1985, pp. 40–41) and Teles da Silva & Peregrine (1988, p. 289), we compute the excess kinetic energy E_k and potential energy E_p due to the presence of waves in each plane, respectively, as

$$\begin{aligned}
E_k &= \int_{-\pi}^{\pi} \int_{-\infty}^{\tilde{y}_0(x)} \frac{1}{2}\{(U_0 - c)^2 + V_0{}^2\} \, dy \, dx - \int_{-\pi}^{\pi} \int_{-\infty}^{0} \frac{1}{2}(\Omega y)^2 \, dy \, dx \\
&= c^2 \int_0^{\pi} \left\{ \left(-y_0 + \frac{1}{2}\frac{\Omega}{c} y_0{}^2\right)(\phi_{0\xi} - x_{0\xi}) + \frac{1}{3}\left(\frac{\Omega}{c}\right)^2 y_0{}^3 x_{0\xi} \right\} d\xi \\
&= -c^2 \int_0^{\pi} \left\{ \left(-y_0 + \frac{1}{2}\frac{\Omega}{c} y_0{}^2\right)(\phi_{0\hat{\vartheta}} - x_{0\hat{\vartheta}}) + \frac{1}{3}\left(\frac{\Omega}{c}\right)^2 y_0{}^3 x_{0\hat{\vartheta}} \right\} d\hat{\vartheta}, \quad (3.10)
\end{aligned}$$

and

$$E_p = \int_{-\pi}^{\pi} \int_0^{\tilde{y}_0(x)} y \, dy \, dx = \int_0^{\pi} y_0{}^2 x_{0\xi} \, d\xi = -\int_0^{\pi} y_0{}^2 x_{0\hat{\vartheta}} \, d\hat{\vartheta}, \tag{3.11}$$

where each energy is non-dimensionalized by $\rho g/k^3$ with ρ being the fluid density.
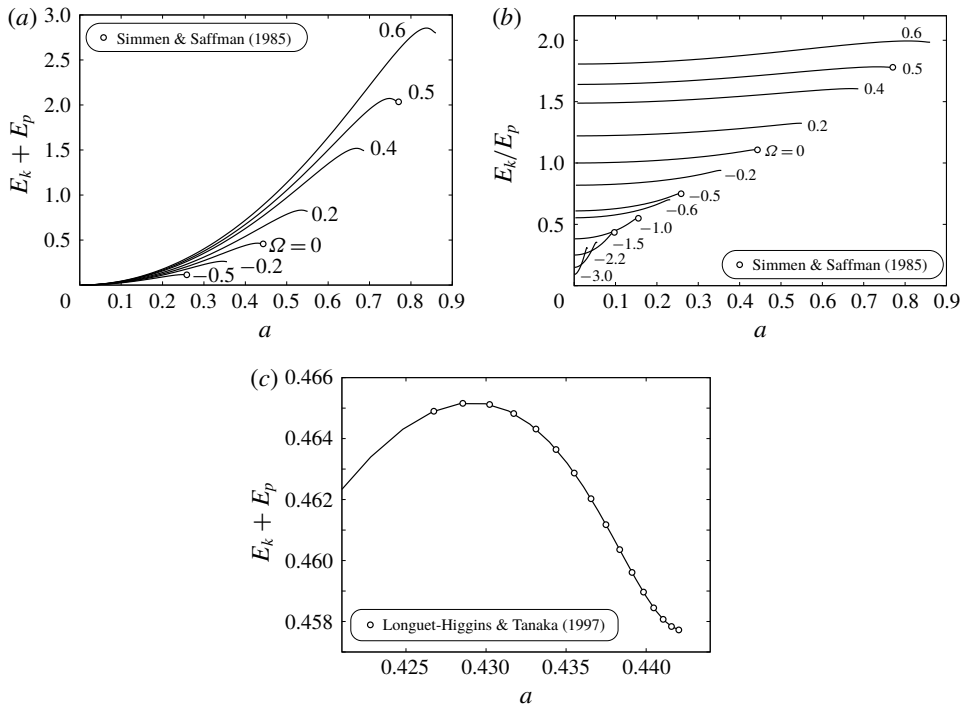
FIGURE 4. Variation of the kinetic energy E_k and the potential energy E_p with the wave steepness a. Circles $\circ$ in (*a*) and (*b*): the computed results for the limiting waves for $\Omega = 0.5$, 0, -0.5, -1 and -1.5 by Simmen & Saffman (1985, table 3 on p. 51), and circle $\circ$ in (*c*): the computed results by Longuet-Higgins & Tanaka (1997, table 4 on p. 55). Each numeral in (*a*) and (*b*) shows the value of shear strength Ω ($N = 256$, $\mu = 0.95$, $0.01 \leqslant \gamma \leqslant 0.95$). (*a*) The sum $E_T = E_k + E_p$. (*b*) The ratio E_k/E_p. (*c*) The sum $E_T = E_k + E_p$ for large-amplitude irrotational waves ($\Omega = 0$).

Figures 4(*a*) and 4(*b*) show some computed results for the total energy $E_T = E_k + E_p$ and the ratio E_k/E_p versus the wave steepness a, respectively, using (3.10) and (3.11), with $N = 256$ and $\mu = 0.95$. It should be noted that E_T attains an extremum at a large amplitude close to that of the limiting wave. This is related to the Tanaka superharmonic instability, as will be shown in §5.1.

The symbols ($\circ$) in figures 3(*a*), 4(*a*) and 4(*b*) show the computed results for the limiting waves by Simmen & Saffman (1985, table 3 on p. 51). Also figures 3(*b*) and 4(*c*) show that the computed results for the wave speed c and the total energy $E_T = E_k + E_p$ of large-amplitude irrotational waves ($\Omega = 0$ and $\gamma \leqslant 0.95$ ($a \leqslant 0.442$)) agree well with those by Longuet-Higgins & Tanaka (1997, table 2 in p. 53 and table 4 on p. 55), respectively. For larger-amplitude waves ($\Omega = 0$ and $\gamma > 0.95$ ($a > 0.442$)), it has been reported that the wave speed c oscillates with the wave steepness a (Longuet-Higgins & Fox 1978; Dyachenko, Lushnikov & Korotkevich 2016; Lushnikov *et al.* 2017), but this phenomenon requires a considerably higher resolution in space than that used in our computations, $N \leqslant 2^9 = 512$. Therefore, we focus on the case of $\gamma \leqslant 0.95$ for stability analysis.

4. Linear stability analysis

This section describes the linear stability analysis of steady wave solutions z_0 and f_0 using the Floquet theory for small disturbances added to z_0 and f_0. For subharmonic disturbances, the ζ-plane is used while the $\hat{\Lambda}$-plane is used for 2π-periodic superharmonic disturbances for a better resolution near the crest.

4.1. *Linearization around steady solutions in the ζ-plane*

For linear stability analysis in the ζ-plane, we add small time-dependent disturbances $z_1(\zeta, t)$ and $f_1(\zeta, t)$ to steady wave solutions $z_0(\zeta)$ and $f_0(\zeta)$ as

$$z(\zeta, t) = z_0(\zeta) + z_1(\zeta, t) \quad \text{and} \quad f(\zeta, t) = f_0(\zeta) + f_1(\zeta, t), \qquad (4.1a,b)$$

and linearize the governing equations with respect to z_1 and f_1. In particular, we look for perturbed solutions of the linearized equations with the exponential growth rate σ in the form

$$z_1(\zeta, t) = \mathrm{e}^{\sigma t} \check{z}_1(\zeta) \quad \text{and} \quad f_1(\zeta, t) = \mathrm{e}^{\sigma t} \check{f}_1(\zeta). \qquad (4.2a,b)$$

Here, $\check{z}_1(\zeta) = \check{x}_1(\xi, \eta) + \mathrm{i}\check{y}_1(\xi, \eta)$ and $\check{f}_1(\zeta) = \check{\phi}_1(\xi, \eta) + \mathrm{i}\check{\psi}_1(\xi, \eta)$ are analytic for $\eta < 0$, and the real part of $\sigma = \sigma_r + \mathrm{i}\sigma_i$ determines the stability of steady solutions. Also note that an analytic function $F(\zeta)$ vanishing as $\eta \to -\infty$ can be represented using its real and imaginary parts at the real axis $\eta = 0$ by

$$F(\zeta) = \mathrm{i}\frac{1}{\pi}\int_{-\infty}^{\infty} \frac{\mathrm{Re}\{F(\zeta = \xi')\}}{\xi' - \zeta}\,\mathrm{d}\xi' = -\frac{1}{\pi}\int_{-\infty}^{\infty} \frac{\mathrm{Im}\{F(\zeta = \xi')\}}{\xi' - \zeta}\,\mathrm{d}\xi'. \qquad (4.3)$$

Then it follows that the real and imaginary parts of perturbed solutions $\check{z}_1(\zeta = \xi)$ and $\check{f}_1(\zeta = \xi)$ at the water surface $\eta = 0$ can be related by

$$\check{x}_1(\xi) = -\mathcal{H}[\check{y}_1(\xi)] \quad \text{and} \quad \check{\psi}_1(\xi) = \mathcal{H}[\check{\phi}_1(\xi)], \qquad (4.4a,b)$$

where the Hilbert transform $\mathcal{H}[\Phi(\xi)]$ of a real-valued function $\Phi(\xi)$ is defined by

$$\mathcal{H}[\Phi(\xi)] = \frac{1}{\pi}\mathrm{PV}\int_{-\infty}^{\infty} \frac{\Phi(\xi')}{\xi' - \xi}\,\mathrm{d}\xi'. \qquad (4.5)$$

Here, PV denotes Cauchy's principal value. The representation (4.1) satisfies the bottom boundary condition (2.15). Substituting (4.1) into the kinematic condition (2.12) and the dynamic condition (2.13) at the water surface $\eta = 0$ in the ζ-plane, we can obtain the linearized equations for $\check{z}_1(\zeta = \xi) = \check{x}_1(\xi) + \mathrm{i}\check{y}_1(\xi)$ and $\check{f}_1(\zeta = \xi) = \check{\phi}_1(\xi) + \mathrm{i}\check{\psi}_1(\xi)$ as

$$\sigma\,(x_{0\xi}\check{y}_1 - y_{0\xi}\check{x}_1) = -(\check{\psi}_{1\xi} + P^{(0)}\check{y}_1 + P^{(1)}\check{y}_{1\xi}), \qquad (4.6)$$

and

$$\sigma\,(x_{0\xi}\check{x}_1 + y_{0\xi}\check{y}_1 - \tilde{J}_0\check{\phi}_1) = Q^{(0)}\check{y}_1 + Q^{(1)}\check{y}_{1\xi} + Q^{(2)}\check{x}_{1\xi} + R^{(0)}\check{\psi}_1 + R^{(1)}\check{\psi}_{1\xi} + R^{(2)}\check{\phi}_{1\xi}, \quad (4.7)$$

where $P^{(\cdot)} = P^{(\cdot)}(\xi)$, $Q^{(\cdot)} = Q^{(\cdot)}(\xi)$ and $R^{(\cdot)} = R^{(\cdot)}(\xi)$ are 2π-periodic functions given by steady solutions z_0 and f_0 as

$$
\left.
\begin{aligned}
&P^{(0)}(\xi) = \frac{\Omega}{c} y_{0\xi}, \quad P^{(1)}(\xi) = \frac{\Omega}{c} y_0, \quad Q^{(0)}(\xi) = \frac{1}{c^2}\tilde{J}_0 + \frac{\Omega}{c}x_{0\xi}, \\
&Q^{(1)}(\xi) = -\frac{y_{0\xi}}{\tilde{J}_0}\left[1 - \left(\frac{\psi_{0\xi}}{\phi_{0\xi}}\right)^2 + \frac{\Omega}{c}2\frac{y_0 x_{0\xi}}{\phi_{0\xi}}\right], \\
&Q^{(2)}(\xi) = -\frac{x_{0\xi}}{\tilde{J}_0}\left[1 - \left(\frac{\psi_{0\xi}}{\phi_{0\xi}}\right)^2 + \frac{\Omega}{c}\frac{y_0 x_{0\xi}}{\phi_{0\xi}}\left\{1 - \left(\frac{y_{0\xi}}{x_{0\xi}}\right)^2\right\}\right], \\
&R^{(0)}(\xi) = -\frac{\Omega}{c}\tilde{J}_0, \quad R^{(1)}(\xi) = -\frac{\psi_{0\xi}}{\phi_{0\xi}}, \quad R^{(2)}(\xi) = 1 + \frac{\Omega}{c}\frac{y_0 x_{0\xi}}{\phi_{0\xi}},
\end{aligned}
\right\}
\tag{4.8}
$$

with $\tilde{J}_0 = J_0/\phi_{0\xi}$ and J_0 being defined by (3.4). Following the Floquet theory, we can write the general solutions of the linear differential equations with periodic coefficients given by (4.6) and (4.7) in the form

$$
\left.
\begin{aligned}
\check{x}_1(\xi) &= \mathrm{e}^{\mathrm{i}p\xi}\sum_{j=-\infty}^{\infty} a_j \mathrm{e}^{\mathrm{i}j\xi}, \quad \check{y}_1(\xi) = \mathrm{e}^{\mathrm{i}p\xi}\sum_{j=-\infty}^{\infty} b_j \mathrm{e}^{\mathrm{i}j\xi}, \\
\check{\phi}_1(\xi) &= \mathrm{e}^{\mathrm{i}p\xi}\sum_{j=-\infty}^{\infty} c_j \mathrm{e}^{\mathrm{i}j\xi}, \quad \check{\psi}_1(\xi) = \mathrm{e}^{\mathrm{i}p\xi}\sum_{j=-\infty}^{\infty} d_j \mathrm{e}^{\mathrm{i}j\xi},
\end{aligned}
\right\}
\tag{4.9}
$$

where $p \in \mathbb{R}$ such that the perturbed solutions are bounded for $-\infty < \xi < \infty$. Using (4.4) and the following property of the Hilbert transform (King 2009, vol. 1, p. 103, equations (3.110) and (3.113))

$$
\mathcal{H}\left[\mathrm{e}^{\mathrm{i}\beta\xi}\right] = \mathrm{i}\,\mathrm{sgn}(\beta)\cdot\mathrm{e}^{\mathrm{i}\beta\xi} \quad \text{with} \quad \mathrm{sgn}(\beta) = \begin{cases} +1 & (\beta > 0) \\ 0 & (\beta = 0) \\ -1 & (\beta < 0) \end{cases},
\tag{4.10a,b}
$$

the coefficients a_j and d_j in (4.9) can be related to b_j and c_j, respectively, by

$$
a_j = -\mathrm{i}\,\mathrm{sgn}(p+j)\cdot b_j \quad \text{and} \quad d_j = \mathrm{i}\,\mathrm{sgn}(p+j)\cdot c_j.
\tag{4.11a,b}
$$

Here, note that a_0 and d_0 for $p=0$ have arbitrariness, as pointed out by Tiron & Choi (2012, p. 406). In this work, these are set to $a_0 = 0$ and $d_0 = 0$ for $p=0$ because they do not affect the linear stability (see appendix A). Substituting (4.9) with (4.11) into (4.6) and (4.7), we get

$$
\left.
\begin{aligned}
\sigma\sum_{j=-\infty}^{\infty} b_j B_{j,p}^{(1b)}(\xi) &= \sum_{j=-\infty}^{\infty}\{b_j A_{j,p}^{(1b)}(\xi) + c_j A_{j,p}^{(1c)}(\xi)\}\mathrm{e}^{\mathrm{i}j\xi}, \\
\sigma\sum_{j=-\infty}^{\infty}\{b_j B_{j,p}^{(2b)}(\xi) + c_j B_{j,p}^{(2c)}(\xi)\} &= \sum_{j=-\infty}^{\infty}\{b_j A_{j,p}^{(2b)}(\xi) + c_j A_{j,p}^{(2c)}(\xi)\}\mathrm{e}^{\mathrm{i}j\xi},
\end{aligned}
\right\},
\tag{4.12}
$$

where $A_{j,p}^{(\cdot)} = A_{j,p}^{(\cdot)}(\xi)$ and $B_{j,p}^{(\cdot)} = B_{j,p}^{(\cdot)}(\xi)$ are 2π-periodic functions given by steady solutions as

$$
\left.
\begin{aligned}
A_{j,p}^{(1b)}(\xi) &= -\{P^{(0)} + \mathrm{i}(p+j)P^{(1)}\}\mathrm{e}^{\mathrm{i}j\xi}, \quad A_{j,p}^{(1c)}(\xi) = |p+j|\mathrm{e}^{\mathrm{i}j\xi}, \\
A_{j,p}^{(2b)}(\xi) &= \{Q^{(0)} + \mathrm{i}(p+j)Q^{(1)} + |p+j|Q^{(2)}\}\mathrm{e}^{\mathrm{i}j\xi}, \\
A_{j,p}^{(2c)}(\xi) &= \mathrm{i}\,\mathrm{sgn}(p+j)\{R^{(0)} + \mathrm{i}(p+j)R^{(1)} + |p+j|R^{(2)}\}\mathrm{e}^{\mathrm{i}j\xi}, \\
B_{j,p}^{(1b)}(\xi) &= \{x_{0\xi} + \mathrm{i}\,\mathrm{sgn}(p+j)y_{0\xi}\}\mathrm{e}^{\mathrm{i}j\xi}, \\
B_{j,p}^{(2b)}(\xi) &= \{-\mathrm{i}\,\mathrm{sgn}(p+j)x_{0\xi} + y_{0\xi}\}\mathrm{e}^{\mathrm{i}j\xi}, \quad B_{j,p}^{(2c)}(\xi) = -\tilde{J}_0\mathrm{e}^{\mathrm{i}j\xi}.
\end{aligned}
\right\}
\tag{4.13}
$$

Furthermore, from periodicity, the coefficients $A_{j,p}^{(\cdot)}$ and $B_{j,p}^{(\cdot)}$ can be expanded in the form of Fourier series as

$$
A_{j,p}^{(\cdot)}(\xi) = \sum_{k=-\infty}^{\infty} A_{k_{j,p}}^{(\cdot)}\mathrm{e}^{\mathrm{i}k\xi} \quad \text{and} \quad B_{j,p}^{(\cdot)}(\xi) = \sum_{k=-\infty}^{\infty} B_{k_{j,p}}^{(\cdot)}\mathrm{e}^{\mathrm{i}k\xi}.
\tag{4.14a,b}
$$

Then, following Galerkin's method (Zhang & Melville 1987), (4.12) can be transformed as

$$
\left.
\begin{aligned}
\sigma \sum_{j=-\infty}^{\infty} B_{k_{j,p}}^{(1b)} b_j &= \sum_{j=-\infty}^{\infty} \left(A_{k_{j,p}}^{(1b)} b_j + A_{k_{j,p}}^{(1c)} c_j \right), \\
\sigma \sum_{j=-\infty}^{\infty} \left(B_{k_{j,p}}^{(2b)} b_j + B_{k_{j,p}}^{(2c)} c_j \right) &= \sum_{j=-\infty}^{\infty} \left(A_{k_{j,p}}^{(2b)} b_j + A_{k_{j,p}}^{(2c)} c_j \right),
\end{aligned}
\right\}
\quad \text{for } \forall k \in \mathbb{Z}.
\tag{4.15}
$$

This can be considered as a generalized eigenvalue problem for the eigenvalue σ and the eigenvector $(\{b_j\}_{j=-\infty}^{\infty}, \{c_j\}_{j=-\infty}^{\infty})$.

4.2. *The method of computation*

For stability analysis of the steady wave solutions numerically obtained in § 3, the water surface $\eta = 0$ and $-\pi \leqslant \xi \leqslant \pi$ for one wavelength in the ζ-plane is divided into $2N$ equal intervals and the sample points on $\eta = 0$ are distributed as $\xi = \xi_m = \pi(m - N)/N$ ($m = 0, 1, \ldots, 2N$). Then, we can numerically obtain the Fourier coefficients in (4.14) using the fast Fourier transform, and each infinite series in (4.14) and (4.15) is approximated by the corresponding partial sum as

$$
\sum_{k=-\infty}^{\infty} \sim \sum_{k=-N}^{N-1} \quad \text{and} \quad \sum_{j=-\infty}^{\infty} \sim \sum_{j=-N}^{N-1},
\tag{4.16a,b}
$$

respectively. Accordingly, the generalized eigenvalue problem (4.15) is reduced to the matrix form

$$
\sigma \boldsymbol{B}_p \boldsymbol{\alpha} = \boldsymbol{A}_p \boldsymbol{\alpha},
\tag{4.17}
$$

with

$$
\boldsymbol{B}_p = \begin{pmatrix} \boldsymbol{B}_p^{(1b)} & \boldsymbol{0} \\ \boldsymbol{B}_p^{(2b)} & \boldsymbol{B}_p^{(2c)} \end{pmatrix}, \quad \boldsymbol{A}_p = \begin{pmatrix} \boldsymbol{A}_p^{(1b)} & \boldsymbol{A}_p^{(1c)} \\ \boldsymbol{A}_p^{(2b)} & \boldsymbol{A}_p^{(2c)} \end{pmatrix}, \quad \boldsymbol{\alpha} = \begin{pmatrix} \boldsymbol{b} \\ \boldsymbol{c} \end{pmatrix},
\tag{4.18a-c}
$$

where $\boldsymbol{A}_p^{(\cdot)} = (A_{k_{j,p}}^{(\cdot)})_{k,j=-N}^{N-1}$ and $\boldsymbol{B}_p^{(\cdot)} = (B_{k_{j,p}}^{(\cdot)})_{k,j=-N}^{N-1}$ are $2N \times 2N$ matrices, and $\boldsymbol{b} = (b_j)_{j=-N}^{N-1}$ and $\boldsymbol{c} = (c_j)_{j=-N}^{N-1}$ are vectors with $2N$ components. In this work, we numerically solved (4.17) using computational routines for eigenvalue problems in LAPACK (http://www.netlib.org/lapack/).

4.3. *Properties of the eigenvalue*

Some characteristic properties of the eigenvalue σ in the generalized eigenvalue problem (4.15) were discussed by Chen & Saffman (1985, p. 128) and Tiron & Choi (2012, p. 407) as follows. First, if σ is the eigenvalue for p, so is $-\overline{\sigma}$ for p, and $-\sigma$ and $\overline{\sigma}$ are the eigenvalues for $-p$, where the overbar denotes the complex conjugate. Next, if σ and $-\overline{\sigma}$ are the eigenvalues for p, then $\overline{\sigma}$ and $-\sigma$ are the eigenvalues for $1 - p$. From these, we consider $p \in [0, 1/2]$ in this work. Note that $p = 0$ and $0 < p \leqslant 1/2$ correspond to super- and sub-harmonic disturbances, respectively.

Furthermore, in the limit of the wave steepness $a \to 0$, we can obtain the eigenvalue $\sigma_{p,j}^{\pm}$ of (4.15) for p and the mode $j \in \mathbb{Z}$ as

$$\sigma_{p,j}^{\pm} = \mathrm{i}\,\mathrm{sgn}(p') \left\{ -|p'| + \frac{\Omega}{2c_0} \pm \sqrt{\frac{|p'|}{c_0{}^2} + \left(\frac{\Omega}{2c_0}\right)^2} \right\} \quad \text{with } p' = p + j \neq 0, \quad (4.19)$$

where the linear wave speed c_0 is defined by (3.8). This will be used to label each branch of the eigenvalue in § 5.

4.4. *Linearization in the $\hat{\Lambda}$-plane for 2π-periodic superharmonic disturbances*

For 2π-periodic superharmonic disturbances ($p = 0$), we can utilize the $\hat{\Lambda}$-plane which is suitable for computation of large-amplitude motion. Similarly to the linearization in the ζ-plane in § 4.1, we write z and f as

$$z(\hat{\Lambda}, t) = z_0(\hat{\Lambda}) + z_1(\hat{\Lambda}, t) \quad \text{and} \quad f(\hat{\Lambda}, t) = f_0(\hat{\Lambda}) + f_1(\hat{\Lambda}, t), \quad (4.20a,b)$$

with

$$z_1(\hat{\Lambda}, t) = \mathrm{e}^{\sigma t}\check{z}_1(\hat{\Lambda}) \quad \text{and} \quad f_1(\hat{\Lambda}, t) = \mathrm{e}^{\sigma t}\check{f}_1(\hat{\Lambda}). \quad (4.21a,b)$$

Here, $\check{z}_1(\hat{\Lambda})$ and $\check{f}_1(\hat{\Lambda})$ are analytic on the unit disk in the $\hat{\Lambda}$-plane. Since $z_0(\hat{\Lambda})$ and $f_0(\hat{\Lambda})$ are given by (B 1), the above representation satisfies the bottom boundary condition (2.21). At the water surface $\hat{\Lambda} = \mathrm{e}^{\mathrm{i}\hat{\vartheta}}$, $\check{z}_1(\hat{\Lambda}) = \check{x}_1(\hat{\vartheta}) + \mathrm{i}\check{y}_1(\hat{\vartheta})$ and $\check{f}_1(\hat{\Lambda}) = \check{\phi}_1(\hat{\vartheta}) + \mathrm{i}\check{\psi}_1(\hat{\vartheta})$ are 2π-periodic with respect to $\hat{\vartheta}$ and can be expanded in the form of Fourier series, similarly to (4.9) and (4.11), as

$$\left. \begin{aligned} \check{x}_1(\hat{\vartheta}) &= \sum_{j=-\infty}^{\infty} \hat{a}_j \mathrm{e}^{\mathrm{i}j\hat{\vartheta}}, \quad \check{y}_1(\hat{\vartheta}) = \sum_{j=-\infty}^{\infty} \hat{b}_j \mathrm{e}^{\mathrm{i}j\hat{\vartheta}}, \\ \check{\phi}_1(\hat{\vartheta}) &= \sum_{j=-\infty}^{\infty} \hat{c}_j \mathrm{e}^{\mathrm{i}j\hat{\vartheta}}, \quad \check{\psi}_1(\hat{\vartheta}) = \sum_{j=-\infty}^{\infty} \hat{d}_j \mathrm{e}^{\mathrm{i}j\hat{\vartheta}}, \end{aligned} \right\} \quad (4.22)$$

with

$$\hat{a}_j = \mathrm{i}\,\mathrm{sgn}(j) \cdot \hat{b}_j \quad \text{and} \quad \hat{d}_j = -\mathrm{i}\,\mathrm{sgn}(j) \cdot \hat{c}_j. \quad (4.23a,b)$$

Here, both $\hat{a}_0$ and $\hat{d}_0$ are set to zero, similarly to a_0 and d_0 for $p = 0$ in (4.11) (see appendix A). The linearized equations (4.6) and (4.7) in the ζ-plane can be transformed to those in the $\hat{\Lambda}$-plane using the change of variables in (2.17). Substituting (4.22) into the linearized equations, we obtain a generalized eigenvalue problem in the same form as (4.15), which may be numerically solved using the method in § 4.2.
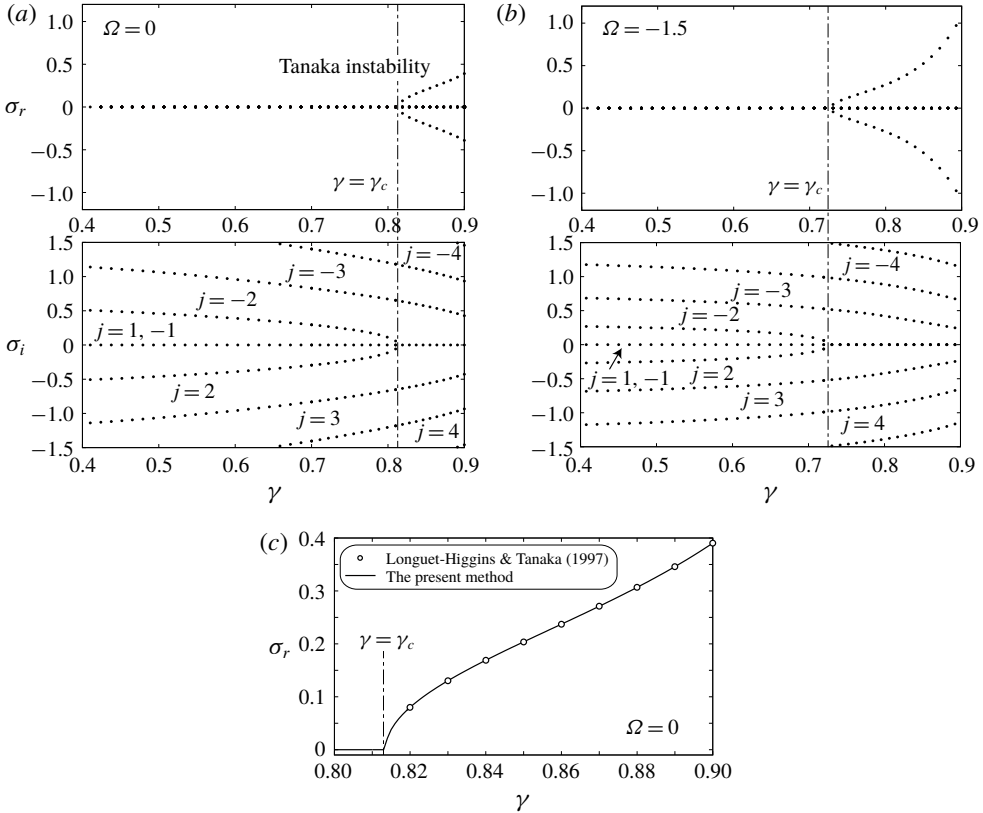
FIGURE 5. Variation of the eigenvalue $\sigma = \sigma_r + \mathrm{i}\sigma_i$ with γ for superharmonic disturbances ($p = 0$, $N = 256$, $\mu = 0.95$). The parameter γ is defined by (3.1). Ω: the shear strength, γ_c: γ at the critical point where the eigenvalues of the modes $j = \pm 2$ vanish and steady waves lose stability and a_c: the wave steepness at $\gamma = \gamma_c$. The mode number j is defined by $\sigma_{p,j}^+$ in (4.19). (*a*) $\Omega = 0$: $\gamma_c \simeq 0.8135$ ($a_c \simeq 0.4292$) and (*b*) $\Omega = -1.5$: $\gamma_c \simeq 0.7274$ ($a_c \simeq 0.0901$). Panel (*c*) compares the growth rate $\sigma_r = \mathrm{Re}\{\sigma\}$ for irrotational waves ($\Omega = 0$) with those by Longuet-Higgins & Tanaka (1997). Solid line —— in (*c*): the present method, and circles ○ in (*c*): Longuet-Higgins & Tanaka (1997, table 4 on p. 55).

5. Numerical examples of linear stability analysis and discussion

This section shows typical computed results for the linear stability of the steady wave solutions, in particular, the variation of eigenvalue $\sigma = \sigma_r + \mathrm{i}\sigma_i$ with the parameter γ or the wave steepness a, for superharmonic ($p = 0$) and subharmonic disturbances ($0 < p \leqslant 1/2$). Each branch of the eigenvalue is labelled using the mode number j of $\sigma_{p,j}^+$ in (4.19) which corresponds to the eigenvalue in the limit of the wave steepness $a \to 0$.

5.1. *Superharmonic instability*

For superharmonic disturbances ($p = 0$), we can numerically investigate linear stability in the $\hat{\Lambda}$-plane, which is suitable for computation of large-amplitude waves, using the method in §§ 4.2 and 4.4. Figures 5–7 show some numerical examples obtained with $N = 256$ and $\mu = 0.95$.
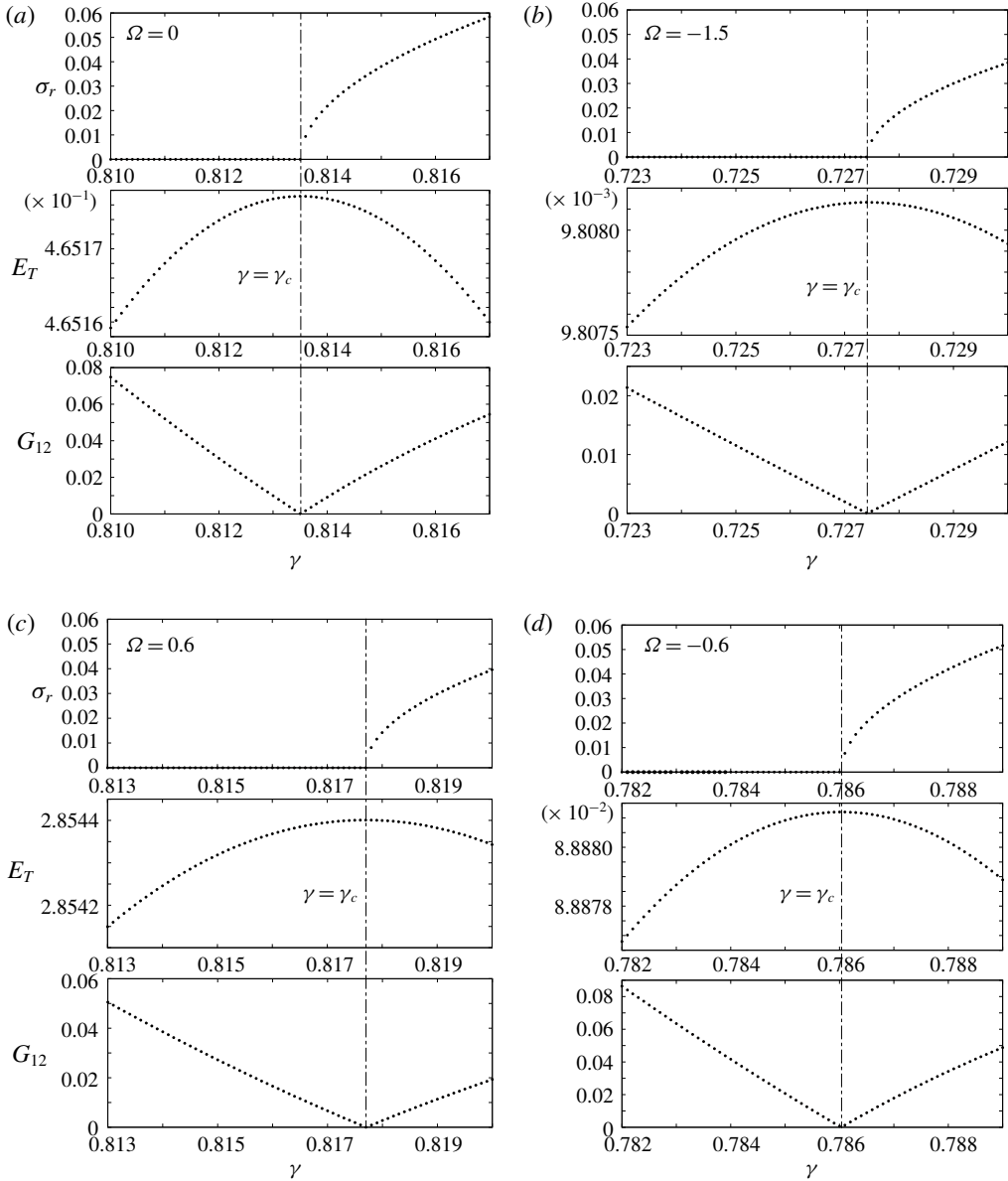
FIGURE 6. Variation of the real part of eigenvalue $\sigma = \sigma_r + i\sigma_i$, the total wave energy $E_T = E_k + E_p$ and the Gramian G_{12} with γ near the critical point $\gamma = \gamma_c$ of the super-harmonic instability of the mode $j = 2$. The parameter γ and the Gramian G_{12} are defined by (3.1) and (5.1), respectively. (a) $\Omega = 0$: $\gamma_c \simeq 0.8135$ ($a_c \simeq 0.4292$), (b) $\Omega = -1.5$: $\gamma_c \simeq 0.7274$ ($a_c \simeq 0.0901$), (c) $\Omega = 0.6$: $\gamma_c \simeq 0.8177$ ($a_c \simeq 0.8377$) and (d) $\Omega = -0.6$: $\gamma_c \simeq 0.7860$ ($a_c \simeq 0.2229$). ($p = 0$, $N = 256$, $\mu = 0.95$).

Figures 5(a) and 5(b) show the variation of eigenvalue $\sigma = \sigma_r + i\sigma_i$ of the mode $j = \pm 1, \pm 2, \pm 3$ and ± 4 with γ for $\Omega = 0$ and -1.5, respectively. Notice that the parameter γ defined by (3.1) increases with the wave steepness a_*, and that the variation of eigenvalues is symmetric with respect to the axes $\sigma_r = 0$ and $\sigma_i = 0$, as
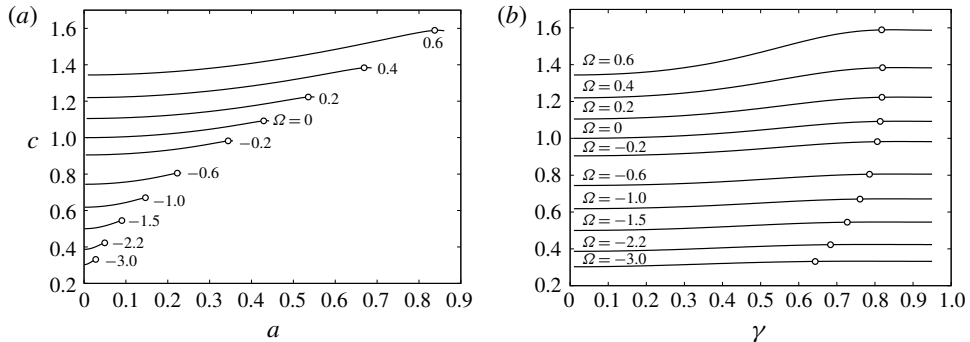
FIGURE 7. Variation of the critical wave steepness a_c and the corresponding parameter γ_c of the superharmonic instability of the mode $j = 2$ with Ω in the (a, c)- and (γ, c)-planes. γ is defined by (3.1), a: the wave steepness, c: the wave speed, Ω: the shear strength and circles $\bigcirc$: the critical point ($p = 0$, $N = 256$, $\mu = 0.95$, $0 \leqslant \gamma \leqslant 0.95$). (a) Variation of a_c with Ω. (b) Variation of γ_c with Ω.

pointed out in §4.3. In addition, figure 5(c) shows that the computed results for the growth rate σ_r for irrotational waves ($\Omega = 0$) in figure 5(a) agree well with those by Longuet-Higgins & Tanaka (1997, table 4 on p. 55).

Figure 5(a) shows that steady irrotational waves ($\Omega = 0$) lose stability at $\gamma = \gamma_c \simeq 0.8135$ (the wave steepness $a = a_c \simeq 0.4292$) due to the superharmonic disturbances of the mode $j = \pm 2$ of which the wavelength is a half that of the steady waves. This result agrees with Tanaka (1983, 1985). This type of superharmonic instability is referred to as the Tanaka instability (MacKay & Saffman 1986), which is characterized by the following three properties: at the critical point $\gamma = \gamma_c$ (or $a = a_c$), (P1) both the real and imaginary parts of eigenvalue $\sigma = \sigma_r + i\sigma_i$ vanish, as shown in figure 5(a), (P2) the total wave energy $E_T = E_k + E_p$ attains an extremum as a function of γ (or a), as shown in figure 6(a), and (P3) the eigenvector $\boldsymbol{\alpha}_1$ of the mode $j = 1$ or -1 is linearly dependent on the eigenvector $\boldsymbol{\alpha}_2$ of the mode $j = 2$ or -2. The property (P3) is due to the fact that the eigenvalue is a multiple root of the characteristic equation and the number of linearly independent eigenvectors is only one at the critical point $\gamma = \gamma_c$ (or $a = a_c$) (Tanaka 1985; Saffman 1985). As shown in Tanaka (1985), we can numerically examine the property (P3) using the Gramian G_{12} of the two eigenvectors $\boldsymbol{\alpha}_1$ and $\boldsymbol{\alpha}_2$, which is defined by

$$G_{12} = |\boldsymbol{\alpha}_1|^2 |\boldsymbol{\alpha}_2|^2 - |(\boldsymbol{\alpha}_1, \boldsymbol{\alpha}_2)|^2, \tag{5.1}$$

where $(\boldsymbol{\alpha}_1, \boldsymbol{\alpha}_2)$ denotes the inner product of $\boldsymbol{\alpha}_1$ and $\boldsymbol{\alpha}_2$. The Gramian G_{12} vanishes if and only if the two eigenvectors $\boldsymbol{\alpha}_1$ and $\boldsymbol{\alpha}_2$ are linearly dependent. Figure 6(a) shows that, for irrotational waves ($\Omega = 0$), the Gramian G_{12} vanishes at the critical point $\gamma = \gamma_c$.

We investigated the variation of this type of superharmonic instability for $-3 \leqslant \Omega \leqslant 0.6$ and $0 \leqslant \gamma \leqslant 0.95$. Figures 7(a) and 7(b) show the variation of the critical points with the shear strength Ω in the (a, c)- and (γ, c)-planes, respectively. From these, we found that, with change of Ω, the critical point moves, but the above three properties (P1), (P2) and (P3) at the critical point $\gamma = \gamma_c$ (or $a = a_c$) still hold, as shown in figures 5(b) and 6(b) for $\Omega = -1.5$ ($\gamma_c \simeq 0.7274$ and $a_c \simeq 0.0901$), figure 6(c) for $\Omega = 0.6$ ($\gamma_c \simeq 0.8177$ and $a_c \simeq 0.8377$) and figure 6(d) $\Omega = -0.6$ ($\gamma_c \simeq 0.7860$ and
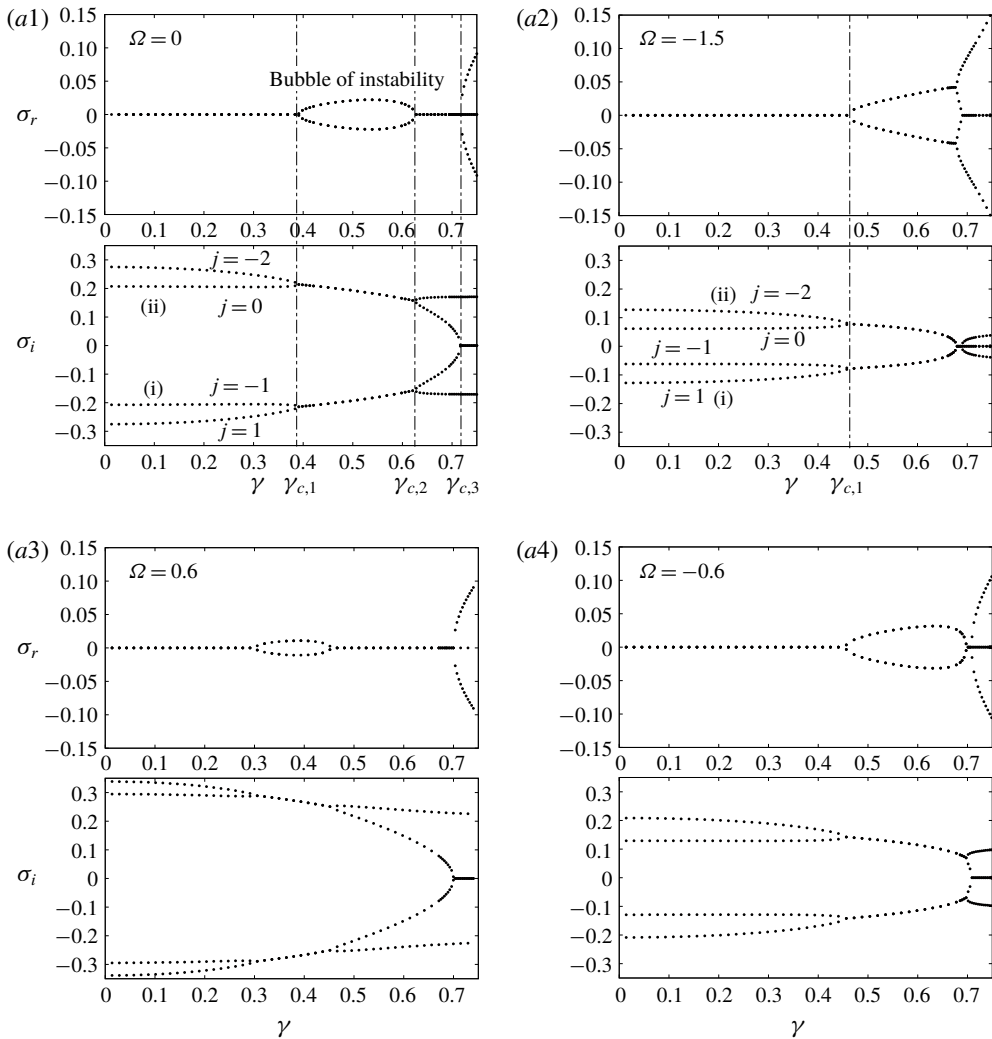
FIGURE 8. For caption see next page.

$a_c \simeq 0.2229$). These agree with the theoretical results by Sato & Yamada (2019). It should be also emphasized that, for downstream propagating waves ($\Omega < 0$), the value of γ_c significantly decreases with increase of $|\Omega|$, and this may be related to the onset of wave breaking due to a sharp change of the slope Θ of the water surface shown in figure 2(b).

5.2. *Subharmonic instability*

For subharmonic disturbances ($0 < p \leqslant 1/2$), whose horizontal scale is longer than that of the steady waves, we can perform a linear stability analysis in the ζ-plane using the method in §§ 4.1 and 4.2. In this section, we focus on the two dominant pairs of eigenvalues, (i) $j = 1$ and -1 and (ii) $j = 0$ and -2, where the mode number j is defined by (4.19). Figures 8 and 9 show some numerical examples for $0 \leqslant \gamma \leqslant 0.75$ with $N = 256$. Note that steady wave solutions are obtained using the method in appendix B with $\mu = 0$, because it is necessary for the fast Fourier transform to
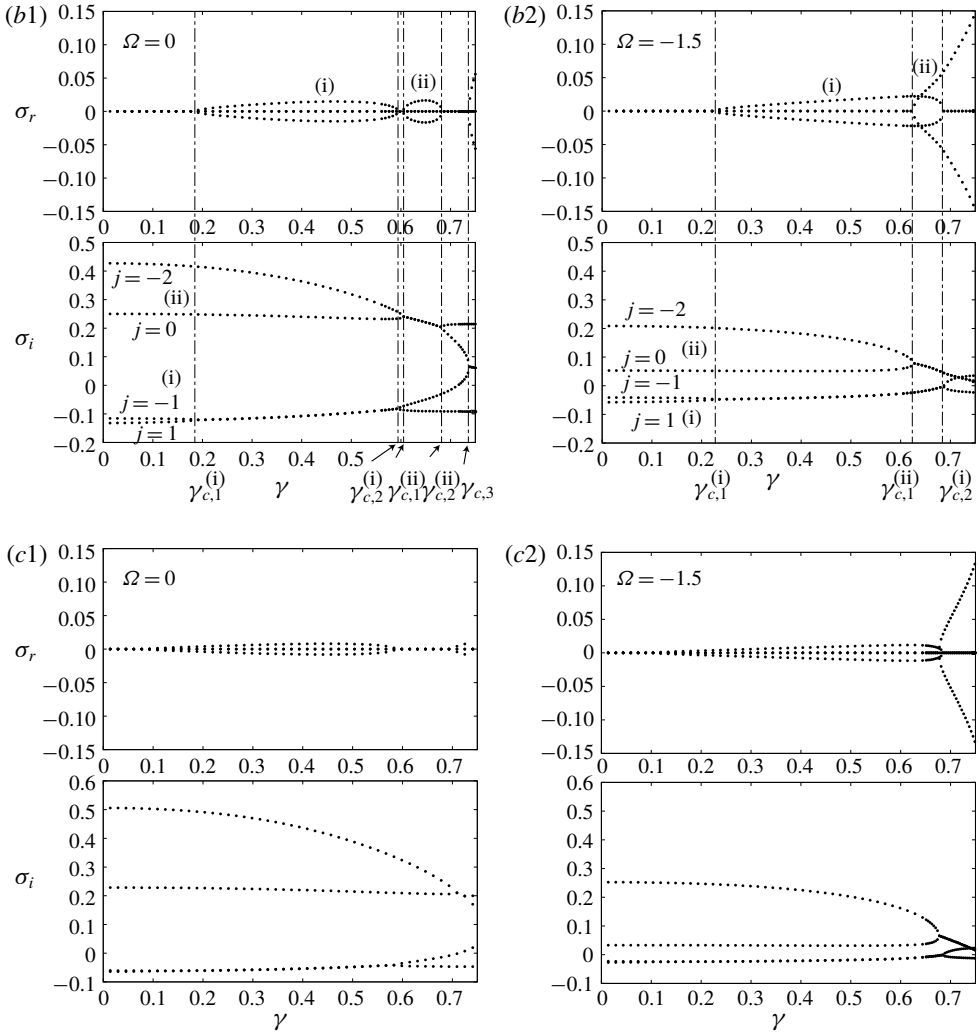
FIGURE 8. (cntd). Variation of the two pairs of eigenvalues $\sigma = \sigma_r + i\sigma_i$, (i) $j = 1$ and -1 and (ii) $j = 0$ and -2, with γ for subharmonic disturbances. The mode number j and the parameter γ are defined by $\sigma_{p,j}^+$ in (4.19) and (3.1), respectively. p: the wavenumber in (4.9) and Ω: the shear strength. Values of γ_c and the corresponding a_c at the critical point are as follows: (a1) $\gamma_{c,1} \simeq 0.3907$ ($a_{c,1} \simeq 0.2286$), $\gamma_{c,2} = 0.6256$ ($a_{c,2} \simeq 0.3672$), $\gamma_{c,3} = 0.7167$ ($a_{c,3} \simeq 0.4049$), (a2) $\gamma_{c,1} \simeq 0.4591$ ($a_{c,1} \simeq 0.0642$). (b1) $\gamma_{c,1}^{(i)} \simeq 0.1853$ ($a_{c,1}^{(i)} \simeq 0.1010$), $\gamma_{c,2}^{(i)} \simeq 0.5947$ ($a_{c,2}^{(i)} \simeq 0.3515$), $\gamma_{c,1}^{(ii)} \simeq 0.6047$ ($a_{c,1}^{(ii)} \simeq 0.3567$), $\gamma_{c,2}^{(ii)} \simeq 0.6828$ ($a_{c,2}^{(ii)} \simeq 0.3925$), $\gamma_{c,3} = 0.7373$ ($a_{c,3} \simeq 0.4115$), (b2) $\gamma_{c,1}^{(i)} \simeq 0.2242$ ($a_{c,1}^{(i)} \simeq 0.0307$), $\gamma_{c,2}^{(i)} \simeq 0.6867$ ($a_{c,2}^{(i)} \simeq 0.0875$), $\gamma_{c,1}^{(ii)} \simeq 0.6252$ ($a_{c,1}^{(ii)} \simeq 0.0827$). (a) $p = 1/2$, (b) $p = 1/4$, (c) $p = 1/8$.

distribute the sample points $\xi = \xi_m$ ($m = 0, 1, \ldots, 2N$) at equal intervals on the water surface in the ζ-plane, as shown in §4.2. Although it was difficult to get highly accurate solutions for $\gamma > 0.75$ with $\mu = 0$, we could catch some typical behaviours of subharmonic instabilities such as a bubble of instability for $-3 \leqslant \Omega \leqslant 0.6$, as shown
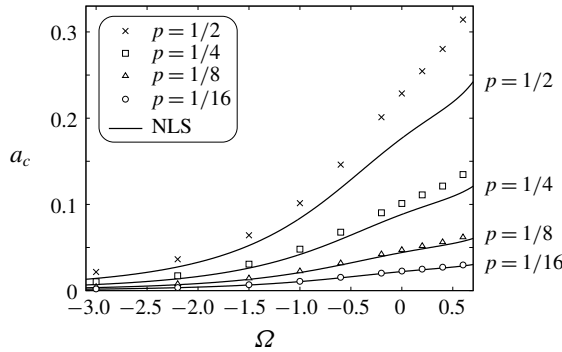
FIGURE 9. Variation of the critical wave steepness a_c at the smallest critical parameter γ_c for subharmonic disturbances with the shear strength Ω. Each mark shows the computed result for the full Euler system using the present method ($\times$: $p = 1/2$, $\square$: $p = 1/4$, $\triangle$: $p = 1/8$, $\circ$: $p = 1/16$). Solid line ———: the weakly nonlinear solution (5.2) of the NLS equation. p: the wavenumber in (4.9) or (5.2).

in this section. Each value of the critical wave steepness a_c and the corresponding parameter γ_c in figure 8 is summarized in the caption of figure 8.

Figure 8(*a*) shows that, for $p = 1/2$, the variation of the eigenvalues with γ is symmetric with respect to the axes $\sigma_r = 0$ and $\sigma_i = 0$, similarly to $p = 0$, as pointed out in §4.3. We can see that each of the two pairs, (i) $j = 1$ and -1 and (ii) $j = 0$ and -2, coalesces at a critical point $\gamma = \gamma_{c,1}$, where the steady waves lose stability. This is the Benjamin–Feir instability. In the case of irrotational waves ($\Omega = 0$), each coalesced eigenvalue is divided into two branches at $\gamma = \gamma_{c,2}$ where the steady waves are re-stabilized, as shown in figure 8(*a*1). This behaviour of the eigenvalues for subharmonic disturbances was found by Longuet-Higgins (1978*b*, 1986) and Branger, Ramamonjiarisoa & Kharif (1986), and called a 'bubble of instability' (MacKay & Saffman 1986). With further increase of γ (or the wave steepness a), a new instability sets in at $\gamma = \gamma_{c,3}$ where the upper branch of the pair (i) collides with the lower branch of another pair (ii).

The behaviour of eigenvalues in figure 8(*a*1) for $\Omega = 0$ and $p = 1/2$ continuously changes with Ω, as shown in figures 8(*a*2), 8(*a*3) and 8(*a*4) for $\Omega = -1.5$, $\Omega = 0.6$ and $\Omega = -0.6$, respectively. With decrease of Ω, the bubble on $\gamma_{c,1} \leqslant \gamma \leqslant \gamma_{c,2}$ moves to the right ($\gamma_{c,1}$ and $\gamma_{c,2}$ increase), and the critical point $\gamma = \gamma_{c,3}$ of the second instability moves to the left ($\gamma_{c,3}$ decreases). With further decrease of Ω, the re-stabilized range $\gamma_{c,2} \leqslant \gamma \leqslant \gamma_{c,3}$ disappears, as shown in figure 8(*a*2) for $\Omega = -1.5$ and $p = 1/2$.

For $0 < p < 1/2$, the two pairs (i) $j = 1$ and -1 and (ii) $j = 0$ and -2 of eigenvalues behave in a quantitatively different, but qualitatively similar, manner, as shown in figures 8(*b*) and 8(*c*) for $p = 1/4$ and $p = 1/8$, respectively. Then the variation of the imaginary part of eigenvalue $\sigma = \sigma_r + i\sigma_i$ is not symmetric with respect to the axis $\sigma_i = 0$. In the case of irrotational waves ($\Omega = 0$), each pair produces a bubble of instability and the two unstable ranges $\gamma_{c,1}^{(i)} \leqslant \gamma \leqslant \gamma_{c,2}^{(i)}$ and $\gamma_{c,1}^{(ii)} \leqslant \gamma \leqslant \gamma_{c,2}^{(ii)}$ appear, as shown in figure 8(*b*1) for $p = 1/4$. Also the third instability occurs at $\gamma = \gamma_{c,3}$ where the two pairs collide, similarly to the case of $p = 1/2$ in figure 8(*a*1). With decrease of Ω, the two bubbles of instability move to the right and overlap each other, as shown in figures 8(*b*2) and 8(*c*2) for $p = 1/4$ and $p = 1/8$ ($\Omega = -1.5$), respectively.

For small-amplitude waves, the critical wave steepness $a = a_c$ corresponding to the smallest critical parameter $\gamma = \gamma_{c,1}^{(i)}$ of the pair (i) $j = \pm 1$ can be approximated using the NLS equation, which was derived by Thomas *et al.* (2012), as

$$a_c = p \cdot \sqrt{\frac{L}{2M}} \quad \text{with} \quad L = \frac{(1 - \tilde{\Omega})^2}{(2 - \tilde{\Omega})^3} \quad \text{and} \quad M = \frac{4 - 10\tilde{\Omega} + 8\tilde{\Omega}^2 - 3\tilde{\Omega}^3}{8(1 - \tilde{\Omega})}, \quad (5.2a\text{-}c)$$

where $\tilde{\Omega}$ (< 1) is defined by (3.9). See appendix C for the NLS equation and the derivation of (5.2). Figure 9 compares the critical wave steepness a_c at $\gamma = \gamma_{c,1}^{(i)}$ in (5.2) with that of the full Euler system which is numerically obtained using the present method for $p = 1/2$, $1/4$, $1/8$ and $1/16$ and $-3 \leqslant \Omega \leqslant 0.6$. It is found that the weakly nonlinear theory using the NLS equation well predicts the critical point only for small-amplitude waves, but fails to do so as the amplitude increases, as expected.

6. Conclusions

We have numerically studied the linear stability of the two-dimensional steady motion of periodic deep-water waves propagating on a linear shear current, whose horizontal velocity varies with depth as $U = c + \Omega y$ in the frame of reference moving with the wave speed c. We have considered both super- and sub-harmonic disturbances and have focused on how the characteristics of instability of steady waves change with the shear strength Ω.

We have used the formulation based on unsteady conformal mapping, which allows us to compute the linear stability of large-amplitude non-overhanging waves with high accuracy. In this formulation, the flow domain is conformally mapped onto the lower half of the ζ-plane or the unit disk in the $\hat{\Lambda}$-plane, as shown in figure 1, where the free surface is fixed onto the real axis or the unit circle, respectively, even if time-dependent disturbances are added to steady waves. The $\hat{\Lambda}$-plane is suitable for accurate computation of the 2π-periodic motion of large-amplitude waves, which requires the high spatial resolution near the wave crest. Following the Floquet theory, perturbed solutions due to small disturbances are expanded in the form of series in the ζ- or $\hat{\Lambda}$-plane, as shown in §4, with the wavenumber $p \in [0, 1/2]$ where $p = 0$ and $0 < p \leqslant 1/2$ correspond to super- and sub-harmonic disturbances, respectively. Substitution of these into the free surface conditions and linearization with respect to small disturbances yield the generalized eigenvalue problem (4.15) for linear stability analysis, which can be numerically solved. We have performed numerical investigation of linear stability for $-3 \leqslant \Omega \leqslant 0.6$ and a wide range of the wave steepness a (or the parameter γ defined by (3.1)), as shown in §5.

For superharmonic disturbances ($p = 0$), it was shown that, even in the presence of a linear shear current ($\Omega \neq 0$), steady waves lose stability at the critical amplitude, where the wave energy is an extremum, similarly to the Tanaka instability for irrotational waves ($\Omega = 0$), as shown in figures 5 and 6. This agrees with the theoretical result by Sato & Yamada (2019). In addition, it was found that the critical wave steepness a_c or the corresponding parameter γ_c changes with Ω and, in particular, γ_c of downstream propagating waves ($\Omega < 0$) significantly decreases with increase of the magnitude $|\Omega|$ of the shear strength, as shown in figure 7.

For subharmonic disturbances ($0 < p \leqslant 1/2$), the variation of eigenvalues with wave amplitude is characterized by the bubble instability, as shown in figure 8. Numerical examples showed that the bubble of instability moves with the shear strength Ω, and

the re-stabilized range disappears for downstream propagating waves ($\Omega < 0$) with a strong shear current, namely a large value of $|\Omega|$. For $p \neq 1/2$, two bubbles of instability are generated and may overlap with change of the shear strength Ω. Also, it was found that the critical wave steepness a_c of the dominant mode for small-amplitude waves can be predicted using the nonlinear Schrödinger equation, as shown in figure 9.

These numerical examples demonstrate that the proposed method using some conformal mapping techniques is helpful to fully understand the complicated structure of the stability of large-amplitude waves on a linear shear current. Nevertheless, the numerical method adopted in this paper needs to be further improved for stability of overhanging waves whose computation requires a considerably large number of Fourier modes, which is a topic for future research.

Acknowledgements

Declaration of interests

The authors report no conflict of interest.

Appendix A. An alternative form of free surface conditions

The left-hand side of the kinematic condition (2.12) and the second term on the left-hand side of the dynamic condition (2.13) can be transformed, respectively, using

$$x_\xi y_t - y_\xi x_t = J \cdot \text{Im} \left\{ \frac{z_t}{z_\zeta} \right\} \quad \text{and} \quad x_\xi x_t + y_\xi y_t = J \cdot \text{Re} \left\{ \frac{z_t}{z_\zeta} \right\}, \quad (A\,1a,b)$$

where J is defined by (2.14). From (4.3), these two can be related using $\text{Re}\{z_t/z_\zeta\} = -\mathcal{H}[\text{Im}\{z_t/z_\zeta\}]$ where the Hilbert transform $\mathcal{H}$ is defined by (4.5). Then it follows that the free surface conditions (2.12) and (2.13) can be rewritten, respectively, as

$$y_t = -\frac{x_\xi}{J} \Psi_\xi + y_\xi \cdot \mathcal{H} \left[\frac{1}{J} \Psi_\xi \right] \quad \text{at } \eta = 0, \quad (A\,2)$$

and

$$\phi_t - \phi_\xi \cdot \mathcal{H} \left[\frac{1}{J} \Psi_\xi \right] + \frac{1}{c^2} y + \frac{1}{2J} (\phi_\xi{}^2 - \psi_\xi{}^2) + \frac{\Omega}{c} \left(\frac{\phi_\xi}{J} y x_\xi - \psi \right) = B(t) \quad \text{at } \eta = 0, \quad (A\,3)$$

where $\Psi_\xi = \psi_\xi + (\Omega/c) y y_\xi$. This alternative form of the free surface conditions (A 2) and (A 3) is suitable for fully nonlinear computation of unsteady waves (Dyachenko *et al.* 1996; Choi & Camassa 1999; Chalikov & Sheinin 2005; Choi 2009; Tiron & Choi 2012; Murashige & Choi 2017), while we can use (2.12) and (2.13) for linear stability analysis without direct evaluation of the Hilbert transform.

In addition, it should be remarked that (A 2) and (A 3) include x_ξ but not x, and that the terms independent of ξ, such as $B(t)$ in (A 3), can be incorporated into ϕ. Hence a_0 and d_0 in (4.9) or $\hat{a}_0$ and $\hat{d}_0$ in (4.22) do not affect linear stability.

Appendix B. The computational method of steady waves in the $\hat{\Lambda}$-plane

From analyticity and symmetry of the solutions and the bottom boundary condition (2.21), steady wave solutions $z_0 = z_0(\hat{\Lambda})$ and $f_0 = f_0(\hat{\Lambda})$ can be expanded and expressed as

$$z_0(\hat{\Lambda}) = \mathrm{i} \log \Lambda(\hat{\Lambda}) + \mathrm{i} \sum_{n=0}^{\infty} \hat{a}_{0n} \hat{\Lambda}^n \quad \text{and} \quad f_0(\hat{\Lambda}) = \mathrm{i} \log \Lambda(\hat{\Lambda}) + \mathrm{i} \sum_{n=0}^{\infty} \hat{b}_{0n} \hat{\Lambda}^n, \quad \text{(B 1a,b)}$$

where $\Lambda = \Lambda(\hat{\Lambda})$ is defined by (2.16), and $\hat{a}_{0n}, \hat{b}_{0n} \in \mathbb{R}$. Taking the real and imaginary parts of (B 1) at the water surface $\hat{\Lambda} = \mathrm{e}^{\mathrm{i}\hat{\vartheta}}$, we have

$$\left.\begin{aligned} x_0(\hat{\vartheta}) &= -\vartheta(\hat{\vartheta}) - \sum_{n=1}^{\infty} \hat{a}_{0n} \sin n\hat{\vartheta}, \\ y_0(\hat{\vartheta}) &= \sum_{n=0}^{\infty} \hat{a}_{0n} \cos n\hat{\vartheta}, \end{aligned}\right\} \quad \text{and} \quad \left.\begin{aligned} \phi_0(\hat{\vartheta}) &= -\vartheta(\hat{\vartheta}) - \sum_{n=1}^{\infty} \hat{b}_{0n} \sin n\hat{\vartheta}, \\ \psi_0(\hat{\vartheta}) &= \sum_{n=0}^{\infty} \hat{b}_{0n} \cos n\hat{\vartheta}, \end{aligned}\right\},$$
$$\text{(B 2)}$$

where $\vartheta = \vartheta(\hat{\vartheta})$ is given by (2.17). Note that the coefficients $\hat{b}_{0n}$ for $n \geqslant 1$ can be determined from $\hat{a}_{0n}$ for $n \geqslant 0$ using $\psi_{0\hat{\vartheta}} = -(\Omega/c) y_0 y_{0\hat{\vartheta}}$ at the water surface, which is given by the kinematic condition (3.2), and that $\hat{b}_{00}$ is not included in the free surface condition (3.5). Thus we can evaluate the free surface condition $\Gamma_1(\hat{\vartheta}) = 0$ in (3.5) by using $\hat{a}_{0n}$ ($n \geqslant 0$), c and B_0. For numerical computation, each infinite series in (B 2) is truncated by its partial sum for $n \leqslant N$, and a finite number of sample points $\hat{\vartheta} = \hat{\vartheta}_m = m\pi/N$ ($m = 0, 1, \ldots, N$) are distributed on the water surface $\hat{\Lambda} = \mathrm{e}^{\mathrm{i}\hat{\vartheta}}$ ($0 \leqslant \hat{\vartheta} \leqslant \pi$) for half-period. Then we may numerically determine the $N + 3$ unknowns $\hat{a}_{0n}$ ($n = 0, 1, \ldots, N$), c and B_0 using Newton's method for

$$\left.\begin{aligned} \Gamma_1(\hat{\vartheta}_m) &= 0 \quad (m = 0, 1, \ldots, N), \\ \Gamma_2 &= (1 - \gamma)^2 \left\{ B_0 - \frac{2}{c^2} y_0(\vartheta = \pi) \right\} - \left\{ B_0 - \frac{2}{c^2} y_0(\vartheta = 0) \right\} = 0, \\ \Gamma_3 &= \int_0^{-\pi} y_0 \, \mathrm{d}x = \int_0^{\pi} y_0 x_{0\hat{\vartheta}} \, \mathrm{d}\hat{\vartheta} = 0, \end{aligned}\right\}, \quad \text{(B 3)}$$

where $\Gamma_1(\hat{\vartheta})$ is defined by (3.3), $\Gamma_2 = 0$ corresponds to the definition of γ in (3.1) and $\Gamma_3 = 0$ is the zero mean level condition (2.1) for steady waves of symmetric profile. In the numerical examples of this paper, the stopping condition of Newton's method was set to

$$\max\{\|\Gamma_1\|_{max}, |\Gamma_2|, |\Gamma_3|\} < 10^{-11}, \quad \text{(B 4)}$$

where $\|\Gamma_1\|_{max} = \max\limits_{m=0,\ldots,N} |\Gamma_1(\hat{\vartheta}_m)|$.

Appendix C. The nonlinear Schrödinger equation for deep-water waves on a linear shear current

Introducing the slow space scale $\tilde{\xi} = \epsilon(x' + c_g t)$ and slow time scale $\tilde{\tau} = \epsilon^2 t$ in the inertial frame (x', y', t) with $x' = x - ct$ and $y' = y$, Thomas *et al.* (2012) derived

the nonlinear Schrödinger (NLS) equation for the complex amplitude $\tilde{a}(\tilde{\xi}, \tilde{\tau})$ of deep-water waves on a linear shear current as

$$i\tilde{a}_{\tilde{\tau}} + c_0(L\tilde{a}_{\tilde{\xi}\tilde{\xi}} + M|\tilde{a}|^2\tilde{a} + K\tilde{a}) = 0, \tag{C 1}$$

where c_g denotes the group velocity given by

$$c_g = \left(\frac{1 - \tilde{\Omega}}{2 - \tilde{\Omega}}\right) c_0 \quad \text{with the linear wave speed } c_0 \text{ defined by (3.8),} \tag{C 2}$$

the small parameter ϵ is the wave steepness, and the constants L and M are defined by (5.2). Note that the propagation direction of waves is opposite to that in Thomas *et al.* (2012), and that the length and the time in (C 1) are scaled by $1/k$ and $1/\sqrt{gk}$, respectively. An arbitrary function $K = K(\tau)$ of τ in (C 1) is related to the choice of the origin of the frame, and set to zero in Thomas *et al.* (2012, (59)). For the linear stability analysis of periodic steady waves satisfying the zero mean level condition (2.1), K is set to

$$K = M_1\tilde{a}_0^2 \quad \text{with a real constant } \tilde{a}_0 \text{ and} \quad M_1 = \frac{\tilde{\Omega}^2(2 - \tilde{\Omega})^2}{8(1 - \tilde{\Omega})}. \tag{C 3}$$

Here, $M = M_0 - M_1$ where M_0 is defined by (3.7). Then it is straightforward to show that

$$\tilde{a} = \tilde{a}(\tilde{\tau}) = \tilde{a}_0 e^{ic_0 M_0 \tilde{a}_0^2 \tilde{\tau}}, \tag{C 4}$$

is a solution of the NLS equation (C 1) and the corresponding wave speed c is given by (3.7) with $a = \epsilon\tilde{a}_0$. Thus (C 4) yields a weakly nonlinear solution for periodic steady waves.

We can analytically investigate linear stability of the weakly nonlinear steady wave solution (C 4) by adding small disturbances $\delta_{\tilde{a}}(\tilde{\xi}, \tilde{\tau})$ and $\delta_{\tilde{c}}(\tilde{\xi}, \tilde{\tau})$ as

$$\tilde{a}(\tilde{\xi}, \tilde{\tau}) = \tilde{a}_0(1 + \delta_{\tilde{a}}) e^{ic_0 M_0 \tilde{a}_0^2 \tilde{\tau} + i\delta_{\tilde{c}}}. \tag{C 5}$$

Substituting this into (C 1) and linearizing it with respect to small $\delta_{\tilde{a}}$ and $\delta_{\tilde{c}}$, we get

$$\left.\begin{array}{l} \dfrac{\partial \delta_{\tilde{a}}}{\partial \tilde{\tau}} + c_0 L \dfrac{\partial^2 \delta_{\tilde{c}}}{\partial \tilde{\xi}^2} = 0, \\[3mm] c_0 L \dfrac{\partial^2 \delta_{\tilde{a}}}{\partial \tilde{\xi}^2} + 2c_0 M \tilde{a}_0^2 \delta_{\tilde{a}} - \dfrac{\partial \delta_{\tilde{c}}}{\partial \tilde{\tau}} = 0. \end{array}\right\} \tag{C 6}$$

This system of linear differential equations has solutions in the form

$$\delta_{\tilde{a}} = \Delta_{\tilde{a}}\, e^{i(\ell\tilde{\xi} - \nu\tilde{\tau})} \quad \text{and} \quad \delta_{\tilde{c}} = \Delta_{\tilde{c}}\, e^{i(\ell\tilde{\xi} - \nu\tilde{\tau})}, \tag{C 7a,b}$$

where $\Delta_{\tilde{a}}$ and $\Delta_{\tilde{c}}$ are constants. Since $\ell\tilde{\xi} = \epsilon\ell(x' + c_g t)$, $\epsilon\ell$ in (C 7) corresponds to the wavenumber p in (4.9). We can determine the stability condition from $\text{Im}\{\nu\} \leqslant 0$ and the condition of non-trivial solutions for (C 6) and (C 7) with $a = \epsilon\tilde{a}_0$ and $p = \epsilon\ell$ as

$$-2M\tilde{a}_0^2 + \ell^2 L \geqslant 0 \quad \text{or} \quad -2Ma^2 + p^2 L \geqslant 0. \tag{C 8a,b}$$

Thus the critical wave steepness a_c of the weakly nonlinear steady wave solution (C 4) is given by (5.2).

REFERENCES

BANNER, M. L. & PHILLIPS, O. M. 1974 On the incipient breaking of small scale waves. *J. Fluid Mech.* **65**, 647–656.

BANNER, M. L. & SONG, J. B. 2002 On determining the onset and strength of breaking for deep water waves. Part II: influence of wind forcing and surface shear. *J. Phys. Oceanogr.* **32**, 2559–2570.

BENJAMIN, T. B. 1962 The solitary wave on a stream with an arbitrary distribution of vorticity. *J. Fluid Mech.* **12**, 97–116.

BRANGER, H., RAMAMONJIARISOA, A. & KHARIF, C. 1986 On the subharmonic instability of very steep deep water gravity wave. *J. Méc. Théor. Appl.* **5**, 515–550.

CHALIKOV, D. & SHEININ, D. 2005 Modeling extreme waves based on equations of potential flow with a free surface. *J. Comput. Phys.* **210**, 247–273.

CHEN, B. & SAFFMAN, P. G. 1985 Three-dimensional stability and bifurcation of capillary and gravity waves on deep water. *Stud. Appl. Maths* **72**, 125–147.

CHOI, W. 2003 Strongly nonlinear long gravity waves in uniform shear flows. *Phy. Rev.* E **68**, 026305.

CHOI, W. 2009 Nonlinear surface waves interacting with a linear shear current. *Maths Comput. Simul.* **80**, 29–36.

CHOI, W. & CAMASSA, R. 1999 Exact evolution equations for surface waves. *J. Engng Mech.* **125**, 756–760.

DOSAEV, A. S., TROITSKAYA, Y. I. & SHISHINA, M. I. 2017 Simulation of surface gravity waves in the Dyachenko variables on the free boundary of flow with constant vorticity. *Fluid Dyn.* **52**, 58–70.

DYACHENKO, A. L. & HUR, V. M. 2019*a* Stokes waves with constant vorticity: folds, gaps and fluid bubbles. *J. Fluid Mech.* **878**, 502–521.

DYACHENKO, A. L. & HUR, V. M. 2019*b* Stokes waves with constant vorticity: I. Numerical computation. *Stud. Appl. Maths* **142**, 162–189.

DYACHENKO, A. L., LUSHNIKOV, P. M. & KOROTKEVICH, A. O. 2016 Branch cuts of Stokes wave on deep water. Part I: numerical solution and Padé approximation. *Stud. Appl. Maths* **137**, 419–472.

DYACHENKO, A. L., ZAKHAROV, V. E. & KUZNETSOV, E. A. 1996 Analytical description of the free surface dynamics of an ideal fluid (canonical formalism and conformal mapping). *Phys. Lett.* A **221**, 73–79.

FRANCIUS, M. & KHARIF, C. 2017 Two-dimensional stability of finite-amplitude gravity waves on water of finite depth with constant vorticity. *J. Fluid Mech.* **830**, 631–659.

FREEMAN, N. C. & JOHNSON, R. S. 1970 Shallow water waves on shear flows. *J. Fluid Mech.* **42**, 401–409.

HSU, H.-C., FRANCIUS, M., MONTALVO, P. & KHARIF, C. 2016 Gravity-capillary waves in finite depth on flows of constant vorticity. *Proc. R. Soc. Lond.* A **472**, 20160363.

KING, F. W. 2009 *Hilbert Transforms*. Cambridge University Press.

LONGUET-HIGGINS, M. S. 1978*a* The instabilities of gravity waves of finite amplitude in deep water. I. Superharmonics. *Proc. R. Soc. Lond.* A **360**, 471–488.

LONGUET-HIGGINS, M. S. 1978*b* The instabilities of gravity waves of finite amplitude in deep water. II. Subharmonics. *Proc. R. Soc. Lond.* A **360**, 489–505.

LONGUET-HIGGINS, M. S. 1986 Bifurcation and instability in gravity waves. *Proc. R. Soc. Lond.* A **403**, 167–187.

LONGUET-HIGGINS, M. S. & FOX, M. J. H. 1978 Theory of the almost-highest wave. Part 2. Matching and analytic continuation. *J. Fluid Mech.* **85**, 769–786.

LONGUET-HIGGINS, M. S. & TANAKA, M. 1997 On the crest instabilities of steep surface waves. *J. Fluid Mech.* **336**, 51–68.

LUSHNIKOV, P. M., DYACHENKO, A. L. & SILANTYEV, D. A. 2017 New conformal mapping for adaptive resolving of the complex singularities of Stokes wave. *Proc. R. Soc. Lond.* A **473**, 20170198.

MACKAY, R. S. & SAFFMAN, P. G. 1986 Stability of water waves. *Proc. R. Soc. Lond.* A **406**, 115–125.

MCLEAN, J. W. 1982 Instabilities of finite-amplitude water waves. *J. Fluid Mech.* **114**, 315–330.

MILNE-THOMSON, L. M. 1968 *Theoretical Hydrodynamics*, 5th edn. Dover.

MIROSHNIKOV, V. A. 2002 The Boussinesq–Rayleigh approximation for rotational solitary waves on shallow water with uniform vorticity. *J. Fluid Mech.* **456**, 1–32.

MOREIRA, R. M. & CHACALTANA, J. T. A. 2015 Vorticity effects on nonlinear wave-current interactions in deep water. *J. Fluid Mech.* **778**, 314–334.

MURASHIGE, S. & CHOI, W. 2017 A numerical study on parasitic capillary waves using unsteady conformal mapping. *J. Comput. Phys.* **328**, 234–257.

MURASHIGE, S. & TANAKA, K. 2015 A new method of convergence acceleration of series expansion for analytic functions in the complex domain. *Japan J. Indust. Appl. Maths* **32**, 95–117.

OKAMURA, M. & OIKAWA, M. 1989 The linear stability of finite amplitude surface waves on a linear shearing flow. *J. Phys. Soc. Japan* **58**, 2386–2396.

OVSHANNIKOV, L. 1974 To the shallow water theory foundation. *Arch. Mech.* **26**, 407–422.

PEREGRINE, D. H. 1976 Interaction of water waves and currents. *Adv. Appl. Mech.* **16**, 9–117.

RUBAN, V. P. 2008 Explicit equations for two-dimensional water waves with constant vorticity. *Phys. Rev.* E **77**, 037302.

SAFFMAN, P. G. 1985 The superharmonic instability of finite-amplitude water waves. *J. Fluid Mech.* **159**, 169–174.

SATO, N. & YAMADA, M. 2019 Superharmonic instability of nonlinear traveling wave solutions in Hamiltonian systems. *J. Fluid Mech.* **876**, 896–911.

SIMMEN, J. A. & SAFFMAN, P. G. 1985 Steady deep-water waves on a linear shear current. *Stud. Appl. Maths* **73**, 35–57.

SWAN, C., CUMMINS, I. P. & JAMES, R. L. 2001 An experimental study of two-dimensional surface water waves propagating on depth-varying currents. Part 1. Regular waves. *J. Fluid Mech.* **428**, 273–304.

TANAKA, M. 1983 The stability of steep gravity waves. *J. Phys. Soc. Japan* **52**, 3047–3055.

TANAKA, M. 1985 The stability of steep gravity waves. Part 2. *J. Fluid Mech.* **156**, 281–289.

TANAKA, M. 1986 The stability of solitary waves. *Phys. Fluids* **29**, 650–655.

TELES DA SILVA, A. F. & PEREGRINE, D. H. 1988 Steep, steady waves on water of finite depth with constant vorticity. *J. Fluid Mech.* **195**, 281–302.

THOMAS, G. P. 1981 Wave-current interactions: an experimental and numerical study. Part 1. Linear waves. *J. Fluid Mech.* **110**, 457–474.

THOMAS, G. P. 1990 Wave-current interactions: an experimental and numerical study. Part 2. Nonlinear waves. *J. Fluid Mech.* **216**, 505–536.

THOMAS, R., KHARIF, C. & MANNA, M. 2012 A nonlinear Schrödinger equation for water waves on finite depth with constant vorticity. *Phys. Fluids* **24**, 127102.

TIRON, R. & CHOI, W. 2012 Linear stability of finite-amplitude capillary waves on water of infinite depth. *J. Fluid Mech.* **696**, 402–422.

VANDEN-BROECK, J. M. 1996 Periodic waves with constant vorticity in water of infinite depth. *IMA J. Appl. Maths* **56**, 207–217.

WAHLÉN, E. 2007 A Hamiltonian formulation of water waves with constant vorticity. *Lett. Math. Phys.* **79**, 303–315.

YAO, A. & WU, C. H. 2005 Incipient breaking of unsteady waves on sheared currents. *Phys. Fluids* **17**, 082104.

ZAKHAROV, V. E. 1968 Stability of periodic waves of finite amplitude on the surface of a deep fluid. *J. Appl. Mech. Tech. Phys.* **2**, 190–194.

ZHANG, J. & MELVILLE, W. K. 1987 Three-dimensional instabilities of nonlinear gravity–capillary waves. *J. Fluid Mech.* **174**, 187–208.